Nature Communications

https://doi.org/10.1038/s41467-026-69796-0

Article in Press

NR2F6 deletion revives CAR-T cell function and induces antigen-agnostic immune memory in solid tumors

Received: 22 November 2024

Accepted: 10 February 2026

Cite this article as: Humer, D., Klepsch, V., Rieder, D. *et al.* NR2F6 deletion revives CAR-T cell function and induces antigen-agnostic immune memory in solid tumors. *Nat Commun* (2026). https://doi.org/10.1038/s41467-026-69796-0

Dominik Humer, Victoria Klepsch, Dietmar Rieder, Isabel Hölzl, Daniel Schreiber, Viktor Lang, Jiří Koutník, Sebastian Peer, Tajana Sajinovic, Viana Wille, Anna Fürst, Dragana Savic, Gabriel Diem, Wilfried Posch, Ira-Ida Skvortsova, Anne Krogsdam, Sieghart Sopper, Sebastian Kobold, Zlatko Trajanoski, Kerstin Siegmund, Nikolaus Thuille, Thomas Gruber, Dominik Wolf & Gottfried Baier

NR2F6 deletion revives CAR-T cell function and induces antigen-agnostic immune memory in solid tumors

Humer Dominik [1 #], Klepsch Victoria[1 * #], Rieder Dietmar[2], Hölzl Isabel[1], Schreiber Daniel[1], Lang Viktor[1], Koutník Jiri[1], Peer Sebastian[1,3], Sajinovic Tajana[1], Wille Viana[1], Fürst Anna[1,4], Savic Dragana[5,6], Diem Gabriel[7], Posch Wilfried[7], Skvortsova Ira-Ida[5,6], Krogsdam Anne[2], Sopper Sieghart[3], Kobold Sebastian[8,9], Trajanoski Zlatko[2], Siegmund Kerstin[1], Thuille Nikolaus[1], Gruber Thomas[1], Wolf Dominik[3] & Baier Gottfried[1 *]

[1]Institute for Cell Genetics, Medical University of Innsbruck, Innsbruck, Austria, [2]Biocenter, Institute of Bioinformatics, Medical University of Innsbruck, Innsbruck, Austria, [3]Department of Internal Medicine V, Haematology & Oncology, Comprehensive Cancer Center Innsbruck and Tyrolean Cancer Research Institute, Medical University of Innsbruck, Innsbruck, Austria, [4]Institute of Molecular Immunology, School of Medicine and Health, Technical University of Munich, Munich, Germany, [5]Tyrolean Cancer Research Institute, Innsbruck, Austria, [6]Department of Therapeutic Radiology and Oncology, Medical University Innsbruck, Innsbruck, Austria, [7]Institute of Hygiene and Medical Microbiology Medical University of Innsbruck, Innsbruck, Austria, [8]Institute for Clinical Pharmacology, Klinikum der Universität München, Munich, Germany, [9]German Cancer Consortium, a partnership between LMU Hospital and the DKFZ, Munich Germany.

 # These authors contributed equally

* *Corresponding authors* ✉ *e-mail: gottfried.baier@i-med.ac.at and victoria.klepsch@i-med.ac.at*

Keywords: CAR-T cell therapy, solid tumors, NR2F6 gene editing, T cell metabolic fitness, Exhaustion resilience, Immunogenic tumor cell death, Epitope spreading, Host memory immunity.

Abstract (149 words):

CAR-T cell therapy is effective in hematologic malignancies but remains challenging in solid tumors owing to antigen heterogeneity and tumor microenvironment-induced exhaustion. Here, gene editing of the nuclear receptor NR2F6 restores CAR-T cell functionality, sustaining a $TCF1^{+}$ progenitor-exhausted phenotype, enhancing metabolic fitness, and preserving cytotoxic potency under chronic antigen exposure. In immunocompetent models, *Nr2f6*-deficient CAR-T cells suppress solid tumor growth and induce robust, polyclonal host antitumor responses that persist after CAR-T clearance, as demonstrated by tumor re-challenge protection. Although infused CAR-T cells disappear within 2 weeks, durable tumor control coincides with epitope spreading and secondary immune responses, likely via dendritic cell reactivation. Protection against antigen-negative tumors and transferable immunity reveal a dual mode of direct cytotoxicity followed by durable immune reprogramming. This broadened host immunity may offset immune escape driven by antigen heterogeneity or loss, establishing NR2F6 inhibition as a promising CAR-T engineering strategy for durable, antigen-agnostic solid-tumor immunotherapy.

Introduction

Chimeric Antigen Receptor (CAR)-T cells combine the antigen recognition ability of antibodies with the cytotoxic effector function of T cells, enabling specific tumor eradication by immune-mediated cytotoxicity independent of the major histocompatibility complex (MHC) [1, 2]. CAR-T cells have transformed the treatment landscape of hematologic malignancies, such as B cell acute lymphoblastic leukemia and diffuse large B cell lymphoma [3, 4, 5]. Despite these successes, CAR-T cell efficacy in solid tumors remains limited. Tumor antigen heterogeneity, loss or downregulation of CAR target antigens, and the immunosuppressive tumor microenvironment (TME) collectively restrict durable anti-tumor responses [6, 7, 8]. Metabolic dysfunction, hypoxia, and nutrient competition within the TME further impair CAR-T cell expansion and persistence by promoting exhaustion [9, 10, 11]. Current approaches such as cytokine "armoring," costimulatory optimization, or checkpoint blockade have achieved encouraging first benefits, but they often lack broad applicability.

Recent work indicates that durable tumor control requires coordinated activity between engineered CAR-T cells and the endogenous immune system. However, the mechanistic understanding of host tumor rejection pathways secondary to CAR-T therapy, particularly the contribution of tumor-derived epitope spreading (ES) that reactivates the non-CAR-T cell immune compartment, remains limited, posing a major challenge for the development of therapies capable of overcoming the profound antigenic heterogeneity characteristic of solid cancers. The phenomenon of ES refers to the induction and secondary amplification of immune responses directed against tumor antigens beyond the original therapeutic CAR target antigen [12, 13]. However, the regulators of this secondary host immune activation remain insufficiently defined. In the context of adoptive cell transfer (ACT), a compelling strategy could be to utilize CAR-T cells for the targeting of one surface-expressed antigen while simultaneously inducing a robust endogenous T cell response against additional tumor antigens. This approach has the potential to effectively address the challenges posed by the high intra-tumor heterogeneity and antigen-loss-mediated immune escape. A growing body of evidence indicates that ES can be elicited and may play a role in the overall therapeutic outcome of cancer immunotherapy [14, 15]. Armored CAR-T cells, engineered to express immunomodulatory mediators like CD40L or FLT3L, were demonstrated to elicit ES to improve anti-tumor immune response of endogenous immunity [16, 17]. In the pre-clinical setting, the majority

of CAR-T studies employed immunodeficient mice, which lack an endogenous T cell response. In immunocompetent murine models, CAR-T therapy appears to possess a limited capacity to elicit ES, particularly in solid tumors [18]. Importantly, the mechanisms by which ES can be promoted during CAR-T therapy remain poorly understood.

Here, we focus our investigation on the role of the orphan nuclear receptor NR2F6, a member of the COUP TF family of nuclear receptors. Acting as an intracellular checkpoint, NR2F6 represses NFAT- and AP-1-dependent cytokine transcription thresholds in effector T cells. It functions mechanistically as a ligand-independent transcriptional repressor that antagonizes the DNA binding of these transcription factors, thereby suppressing the expression of key pro-inflammatory cytokines, including IL-2, IFNγ, TNF, IL-17, and IL-21 [19, 20, 21]. The activity of NR2F6 is tightly controlled by PKC-mediated phosphorylation, which modulates chromatin association and transcriptional repression [21]. Through this molecular brake, NR2F6 maintains immune homeostasis and prevents excessive effector differentiation into highly activated T lymphocyte subsets [19, 20, 21]. Inhibition of *Nr2f6* enhances also NK cell effector function [22] and improves pathogen clearance in a preclinical Listeria monocytogenes model [23]. Together with our previous studies identifying NR2F6 as an intracellular immune checkpoint in the effector T cell compartment [24, 25], these findings establish NR2F6 as a promising therapeutic target for enhancing anti-tumor immunity. Moreover, NR2F6 expression in melanoma cells contributes to immune evasion and tumor progression, underscoring its dual role in the tumor microenvironment [26]. These findings emphasize the translational relevance of targeting NR2F6 in cancer immunotherapy and provide a rationale for exploring *Nr2f6*-edited CAR-T cells in solid tumor models.

We therefore hypothesized that deletion of *Nr2f6* could reprogram CAR-T cells toward a metabolically fitter, less exhausted state, capable of initiating robust adaptive immune amplification through tumor antigen cross priming and epitope spreading. Here, we examine the consequences of *Nr2f6* deletion in CAR-T cells directed against solid, syngeneic tumors in fully immunocompetent mice. We demonstrate that CRISPR/Cas9 engineered, *Nr2f6*-deficient CAR-T cells confer robust anti-tumor cytotoxicity and achieve superior tumor control compared with controls. Importantly, these cells maintain a sustained $TCF1^{+}$ progenitor state, display enhanced metabolic resilience, and preserve potent effector functions under chronic antigen stimulation. As a direct consequence, *Nr2f6* edited CAR-T cells provoke secondary, polyclonal host immune

responses through immunogenic tumor cell death and activation of antigen presenting cell-mediated epitope spreading that extends beyond the CAR targeted antigen.

Using CRISPR/Cas9-engineered CAR-T cells in immunocompetent mouse models, we demonstrate that *Nr2f6* deletion establishes durable antitumor immunity marked by sustained $TCF1^{+}$ progenitor states, heightened cytokine production under chronic stimulation, and dendritic-cell–dependent epitope spreading (ES). This integrated mechanism positions NR2F6 inhibition as a pivotal link between restored CAR-T-cell cytotoxicity within the immunosuppressive tumor microenvironment and the induction of antigen-agnostic host immune memory. To our knowledge, this work provides the first experimental framework showing that gene editing can transform CAR-T cells into robust catalysts of systemic, polyclonal antitumor immunity capable of overriding adaptive resistance in solid tumors.

Collectively, these findings position NR2F6 as a tractable metabolic checkpoint and articulate a conceptual blueprint for CAR-T engineering strategies that enhance secondary, polyclonal, antigen-agnostic host immune priming against additional tumor antigens beyond the CAR-targeted antigen, thereby overcoming tumor antigen heterogeneity as a central barrier to effective solid-tumor immunotherapy.

Results

CRISPR/Cas9-mediated *Nr2f6* deletion enhances CAR-T efficacy across independent solid tumor models

Based on our previously published results, we hypothesized that depletion of *Nr2f6* may improve CAR-T cell therapy in solid tumors. To test our hypothesis, we used an investigational second-generation CAR, directed against murine EpCAM, and a solid syngeneic tumor model involving the pancreatic ductal adenocarcinoma cell line Panc02 engineered to overexpress EpCAM *in vivo* [27]. This 28ζ CAR consists of a scFv fragment, derived from the αEpCAM antibody clone G8.8, fused to an intracellular CD28 as well as CD3ζ domain connected *via* a CD8 hinge and a CD28 transmembrane region (Fig1A). For translational reasons, we edited the *Nr2f6* gene in primary mouse $CD8^+$ T cells using CRISPR/Cas9. Synthetic guide (g)RNAs targeting the *Nr2f6* locus were introduced by electroporation into Cas9 transgenic (Cas9tg) $CD8^+$ T cells. *Nr2f6* gene editing efficiency was determined by tracking of indels by decomposition (TIDE) analysis: *Nr2f6*.gRNA03 frequently yielded an efficiency >90%, whereas *Nr2f6*.gRNA04 was less efficient with 40% (Suppl.Fig4A). Of note, and of potential clinical relevance, we have previously demonstrated that even partial loss of *Nr2f6*, as seen in heterozygous knockout mice, is sufficient to elicit a robust anti-tumor phenotype [24]. This indicates that full genetic inactivation may not be required and that haploinsufficiency alone can drive significant therapeutic effects. To assess the anti-tumor efficacy of non-targeting control (NTC) and $Nr2f6^{crispr-/-}$ CAR-T cells, we inoculated fully immunocompetent wild type mice subcutaneously with 70% antigen-positive $1x10^6$ Panc02-EpCAM cells to introduce surrogate heterogeneity. Two days later, once the tumors had become established, we treated the mice intravenously with 3.6×10^6 CAR-T cells (Fig1B). Treatment of tumor-bearing mice with $Nr2f6^{crispr-/-}$ CAR-T cells resulted in reduced tumor growth and prolonged overall survival compared to control animals treated with *NTC* CAR-T cells (Fig1C-E). Notably, 55% (5/9) of animals in the knockout-treated group showed complete remission after tumor challenge versus 9% (1/11) in the NTC group. Similar results could be obtained in $Nr2f6^{crispr-/-}$ CAR-T-treated tumor bearing mice using an independent non-sequence overlapping gRNA indicating that indeed the knockout of *Nr2f6* is responsible for the superior anti-tumor response (Suppl.Fig4B). *Nr2f6* gene-edited polyclonal non-CAR transduced $CD8^+$ T cells alone failed to

induce an anti-tumor immune response in this harsh solid tumor model, suggesting that potent tumor rejection is dependent on both, CAR expression and deletion of *Nr2f6* (Suppl.Fig4C).

To demonstrate broader applicability, we employed two independent CAR-T mouse models expressing an anti-human EGFR 28ζ CAR, together with syngeneic B16-F10 and MC38 tumor cells transduced with human EGFR (hereafter referred to as B16-F10-hEGFR and MC38-hEGFR). In both additional syngeneic tumor models, *Nr2f6*-depleted CAR-T-treated animals exhibited superior tumor control and prolonged survival compared with NTC CAR-T recipients (Suppl.Fig2A–G). These findings underline the broader relevance of *Nr2f6*-modified CAR-T cells, which achieve more effective and durable tumor clearance across distinct solid-tumor models.

Several clinical studies have highlighted the importance of CAR-T cell persistence regarding clinical outcome [28, 29]. Therefore, we challenged Ly5.1$^+$ mice with Panc02-EpCAM tumors and treated them with Ly5.2$^+$ CAR-T cells to track transferred CAR-T cells. On day 3 after adoptive CAR-T cell transfer (ACT), we observed an increased fraction of *Nr2f6*$^{crispr-/-}$ CAR-T cells within the tumor compared to NTC-treated controls (Fig1F). Notably, flow cytometry analysis revealed that *Nr2f6*-depleted CAR-T cells in the tumor-draining lymph node (tdLN) express elevated levels of TCF1 protein (Fig1G, H), a key transcription factor shown to regulate T cell memory formation and stemness [30, 31]. To assess their cytotoxic phenotype, we re-stimulated NTC and *Nr2f6*$^{crispr-/-}$ CAR-T cells from spleens of tumor-bearing mice *ex vivo* with target tumor cells. *Nr2f6*-modified CAR-T cells produced significantly higher amounts of interferon gamma (IFNγ) and granzyme B (GrzB) compared to controls (Fig1I, J), supporting their enhanced effector function. Of note, however, we did not observe long-term persistence of the CAR-T cells as they were undetectable in the spleen of all animals after day 13, regardless of treatment regimen (Suppl.Fig4D). Hence, we hypothesized that ACT with *Nr2f6*-modified (but not control) CAR-T cells might have facilitated a secondary immune response that appears to enable durable tumor rejection. Of note, and focusing on CAR persistence, some reports highlight the crucial role of CD4$^+$ T cells promoting and sustaining CAR-T cell responses in long term responders [28]. We transferred a mixture of CD8$^+$ and CD4$^+$ *Nr2f6*$^{crispr-/-}$ CAR-T cells to evaluate the impact of CD4$^+$ T cell help but were unable to observe a beneficial effect on tumor growth comparing to CD8$^+$ CAR-T cell only therapy (Suppl.Fig2H-K). Surprisingly, we could observe a comparable CD8$^+$ only phenotype when transferring CD4$^+$ *Nr2f6*$^{crispr-/-}$ CAR-T cells (Suppl.Fig9). Collectively, these results suggest

that CRISPR/Cas9-mediated depletion of *Nr2f6* in $CD8^+$ CAR-T cells substantially improves therapeutic efficacy.

Nr2f6 deletion enhances CAR-T cytotoxicity

To explain our observed *in vivo* phenotype, we went back to phenotypically investigate the difference between wild type (WT) and *Nr2f6*-deficient CAR-T cells. *Nr2f6* mRNA expression is markedly induced in WT T cells during CAR-T production (Suppl.Fig5A). This observation is of functional relevance, as NR2F6 is a negative T cell regulator that is induced upon TCR stimulation. That prompted us to test potential functional consequences of *Nr2f6* depletion in CAR-T cells *in vitro* that may explain the superior therapeutic *in vivo* phenotype. We did not observe any differences in CAR transduction efficiency (Fig2A) or expansion of *Nr2f6*$^{-/-}$ or WT $CD8^+$ T cells during CAR-T cell production (Suppl.Fig5B). Upon acute stimulation of CAR-T cells with Panc02-EpCAM at an effector to target (E:T) ratio of 5:1 overnight, *Nr2f6*$^{-/-}$ CAR-T cells produced higher levels of IFNγ, reflecting the results obtained from *ex vivo* stimulation (Fig2B). To test whether this is a 28ζ CAR-dependent phenotype, we also stimulated αEpCAM CAR-T cells harboring a 41BB signaling domain with Panc02-EpCAM. Consistently with our previous results, *Nr2f6*-modified BBζ CAR-T cells produce more IFNγ compared to WT controls (Suppl.Fig5C). We next asked if this augmented production is maintained during chronic stimulation. Loss of effector cytokine production represents a hallmark of exhaustion, which appears to be one of the major hurdles of optimal CAR-T cell efficacy against solid tumors *in vivo* [32, 33]. To address this issue, we established an *in vitro* chronic tumor antigen stimulation assay forcing 28ζ CAR-T cells into an exhaustion-like state (Fig2C, Suppl.Fig5D). Assessing different E:T ratios, 5:1 particularly induced the expression of multiple inhibitory receptors in WT CAR-T cells, frequently found in exhausted T cells (Suppl.Fig5D). Of note, chronic stimulation similarly increased *Nr2f6* mRNA levels in WT CAR-T cells in this setting (Suppl.Fig5E). *Nr2f6*$^{-/-}$ CAR-T cells challenged over multiple rounds with Panc02-EpCAM cells showed superior killing capacity (Fig2D) accompanied by increased IFNγ and GrzB secretion when compared to WT CAR-T cells (Fig2E, F). Additionally, we subjected CAR-T cells to bulk RNA sequencing (RNAseq) on day 8 during chronic stimulation to elucidate transcriptional differences. Gene ontology (GO) overrepresentation analysis of differentially expressed genes (DEGs) revealed enrichment of T cell

activation and cytotoxic signaling pathways, supporting the enhanced antitumor potential of *Nr2f6*-modified CAR-T cells (Fig2G, H).

To exclude off-target killing *via* death receptors like Fas or NKG2D, we co-cultured wild type CAR-T cells with Panc02 tumor cells expressing or not expressing the CAR-targeted antigen EpCAM. We could confirm that only CAR antigen-positive Panc02 cells were killed in a CAR-dependent manner (Suppl.Fig5F). CAR-T cells were shown to primarily kill their targets in a perforin-granzyme B-dependent manner, which in turn leads to activation of pro-apoptotic caspase 3, but also to cleavage of gasdermin E (GSDME) ultimately resulting in tumor cell death. The active amino-terminal domain of GSDME has membrane pore-forming properties converting non-inflammatory apoptosis into a highly immunogenic form of cell death, termed pyroptosis [34, 35]. To further validate the superior killing phenotype of *Nr2f6*$^{-/-}$ CAR-T cells at the tumor target cell level, we assessed GSDME clipping on day 4 of chronic stimulation using Western blot. Quantification revealed that tumor cells co-cultured with *Nr2f6*-modified CAR-T cells showed a significantly increased GSDME clipping activity of full-length GSDME to N-GSMDE when compared to wild type CAR-T cells (Fig2I). Together, these data provide convincing evidence that *Nr2f6* deletion in CAR-T cells enhances their anti-tumor potency, which is associated with enhanced cytotoxic activity against solid tumors *in vitro* and preserved functionality during repetitive stimulation.

_Nr2f6_ ablation preserves TCF1^{+} stem-like progenitors and metabolic fitness

Next, we set out to determine a deeper phenotypic characterization of our CAR-T cells during chronic stimulation *in vitro*. Loss of *Nr2f6* resulted in a notable increase in the number of CD62L-CD44 double-positive cells (Fig3A), with a shift toward a central memory (CM)-like phenotype. We next asked whether this increase in double-positive CAR-T cells with persistent cytokine secretion would also result in a difference in the manifestation of exhaustion. Indeed, when we examined PD-1^{+} CAR-T cells, we identified a significant difference in the ratio of CD8^{+} progenitor exhausted T cells (Tpex, Ly108^{+}Tim3^{-}) to terminally exhausted T cells (Ttex, Ly108^{-}Tim3^{+}) (Tpex/Ttex) (Fig3B) as another underlying mechanism for the benefit of *Nr2f6*-modified CAR-T cells. In addition, FACS analysis revealed that *Nr2f6*$^{-/-}$ CAR-T cells expressed more TCF1 on day 4 of co-culture (Fig3C) consistent with previously published data showing that Tpex cells remain

TCF1 positive [36]. Collectively, these data demonstrate that *Nr2f6* loss is associated with decreased terminal differentiation and increased expression of TCF1 maintaining a progenitor exhausted state.

To maintain their cytotoxic machinery, especially in the TME, $CD8^+$ T cells require high metabolic activity. Therefore, we next assessed the metabolic profile of *Nr2f6*-deleted and WT CAR-T cells during chronic stimulation using the Seahorse Cell Mito Stress Test on day 4 of co-culture, when we observed the greatest difference in Tpex/Ttex ratio. Analysis showed that *Nr2f6*-modified CAR-T cells exhibited a superior resilience towards stress, which is paralleled by higher basal and maximum oxygen consumption rates (OCR) when compared to WT CAR-T cells (Fig4A). In addition, knockout CAR-T cells have a higher extracellular acidification rate (ECAR) due to an increased glycolytic potential (Fig4B). Consistent with this phenotype, GO overrepresentation analysis of bulk RNAseq data from day 4 of chronic stimulation showed enrichment in key metabolic pathways (Fig4C-D). Gene set enrichment analysis (GSEA) between knockout and WT CAR-T cells revealed that gene sets associated with OXPHOS, glycolysis and fatty acid oxidation (FAO) were significantly up-regulated in *Nr2f6*-modified CAR-T cells (Fig4E). Collectively, all *in vitro* characterization results indicate that *Nr2f6* knockout in CAR-T enhances performance by increasing cytotoxic capacity, maintaining effector cytokine production and preventing terminal exhaustion/differentiation, thereby preserving a pool of Tpex cells *in vitro*. Mechanistically, loss of the transcription factor NR2F6 leads to metabolic reprogramming, increasing both OXPHOS and glycolysis potential to meet energy demands during repetitive stimulation.

_Nr2f6_ ablation facilitates immunogenic tumor cell death and activation of host immunity

Since we did not use lymphodepletion and because CAR-T cells disappeared over time, we next concentrated on better understanding the long-term cancer control triggered by ACT of *Nr2f6*-modified CAR-T cells with a particular focus on the role of the endogenous immune system. More specifically, we determined whether $Nr2f6^{crispr-/-}$ CAR-T cells boost the endogenous immune system by "warming up the TME" leading to ES. Immunogenic cell death (ICD) is known to promote priming and activation of the endogenous immune system, ultimately resulting in polyclonal and durable tumor cell clearance. To test this hypothesis of an ES-mediated secondary host immune activation event by the *Nr2f6*-modified CAR-T treatment regimen, we injected immunodeficient $Rag1^{-/-}$ recipients, who lack an endogenous adaptive immune compartment, with

Panc02-EpCAM followed by treatment with *Nr2f6*$^{crispr-/-}$ or *NTC* CAR-T cells two days later (Fig5A). In strict contrast to the results obtained with immunocompetent wild type recipients (shown above in Fig1C-E), treatment with *Nr2f6*-modified CAR-T cells did not result in a tumor growth inhibition or a survival benefit (Fig5B, C). The loss of therapeutic effects in *Rag1*$^{-/-}$ again indicates that an endogenous adaptive immune cell response is required for the superior tumor control mediated by *Nr2f6*-modified CAR-T cells, promoting a secondary response by the endogenous immune system, which is present only in immunocompetent WT mice.

To further validate these findings, we isolated splenocytes from *Nr2f6*$^{crispr-/-}$ and *NTC* CAR-T-receiving immunocompetent WT animals 8 days after tumor injection and subjected them to FACS analysis (Fig5D). Analysis revealed that immunocompetent mice treated with *Nr2f6*$^{crispr-/-}$ CAR-T cells showed an enrichment of conventional dendritic cell type1 (cDC1) cells in the spleen (Fig5E), as well as increased IL-12p40 in the serum, the master cytokine to prime T cell effector function (Fig5H). cDC1 and their cytokines have been shown to be essential for anti-tumor immunity, primarily by priming and supporting the differentiation of cytotoxic T lymphocytes (CTLs) [37]. To further support our hypothesis that the secondary host immune response is triggered by the superior cytotoxic activity of *Nr2f6*-modified CAR-T cells due to ES, we performed ELISpot experiments. In the absence of the CAR-targeted tumor antigen EpCAM, polyclonal anti-Panc02 T cell responses were evaluated. Using previously established Panc02 neoantigens [38], an ELISpot assay was performed using isolated endogenous CD3$^+$ T cells from spleens from tumor-bearing animals on d19 after treatment with either NTC or *Nr2f6*$^{crispr-/-}$ CAR-T cells (Fig.5D). The host CD3$^+$ T cells were stimulated *ex vivo* with DCs loaded with either peptide pools of the described Panc02 neoantigens (Suppl.Table1), primary tumor samples or Panc02 cell line lysates. As a result, we were able to validate DC-mediated ES via T cell priming. Treatment with *Nr2f6*$^{crispr-/-}$ CAR-T cells, but not, or at least to a much lesser extent, with *NTC* CAR-T cells, resulted in a significantly enhanced endogenous polyclonal T cell response as evidenced by increased GrzB production (Fig5G, H). Therefore, this durable tumor control observed after the apparent disappearance of CAR-T cells can be explained by ES and the subsequent induction of a secondary, tumor-antigen–specific host T cell response.

To confirm this host T cell response in more detail, we focused on CD8$^+$ T cells, because they were shown to be the most relevant cell type for anti-cancer adaptive immunity. Therefore, we

again treated immunocompetent Panc02-EpCAM tumor-bearing mice with either NTC or *Nr2f6*$^{crispr-/-}$ CAR-T cells and subjected spleens, tdLNs and tumors to FACS analysis 3 days after ACT. We discovered an increased fraction of endogenous CD8$^+$ T cells in the spleen of *Nr2f6*-modified CAR-T-treated animals (Suppl.Fig3A). Furthermore, these CD8$^+$ T cells showed an attenuated exhaustion phenotype (more Ly108$^+$Tim3$^-$ cells) compared to CD8$^+$ T cells from NTC receiving mice (more Ly108$^-$Tim3$^+$ cells) (Suppl.Fig3B-E). Importantly, *Nr2f6*-depleted CAR-T-treated mice exhibited an increased Tpex/Ttex ratio among CD8$^+$ T cells in the spleen compared to control-treated animals (Suppl.Fig3D). Analysis further revealed that *Nr2f6*$^{crispr-/-}$ CAR-T-treated animals showed an increased number of NK cells as well as increased IFNγ-producing endogenous CD8$^-$ T cells in the tdLN compared to control-treated mice (Suppl.Fig3F, G). Since recruitment of immune cells is dependent on cytokines and chemokines, we performed a cytokine array assay using lysates from whole spleens. The assay revealed that several inflammatory cytokines (IL13, MIP-1β, MIP-2, IL-12) were elevated in *Nr2f6*$^{crispr-/-}$ CAR-T-treated mice compared to controls (Suppl.Fig3H). Overall, we observe an apparently facilitated cooperative anti-tumor effect of *Nr2f6*-modified CAR-T therapy and endogenous innate and adaptive immune cell compartments, initiating a cascade of endogenous immune priming.

Epitope spreading facilitates antigen-agnostic durable immunity

Crucially, to ascertain whether *Nr2f6*$^{crispr-/-}$ CAR-T cell therapy promotes ES and subsequently the activation of the endogenous immune system *in vivo*, we simultaneously challenged the *Nr2f6*-modified CAR-T-treated complete responder (CR) cohort with EpCAM-positive and EpCAM-negative Panc02 tumors injected in the right and left flank, respectively (Fig6A). In line with our hypothesis, each *Nr2f6*-modified CAR-T complete-responder mouse eradicated both EpCAM-positive and EpCAM-negative Panc02 tumors (Fig6B) and showed superior survival compared with tumor-bearing control mice (Fig6C). It is important to note that this secondary immune response apparently was EpCAM independent, which provides strong evidence in support of ES as the underlying process in driving effective polyclonal host anti-tumor immune responses. Consistently, we hypothesized that cDC1-mediated ES may have occurred in the *Nr2f6*$^{crispr-/-}$ CAR-T treated CR cohort as a mechanistic basis for the efficient rejection of EpCAM-negative tumors. We again exposed the CR cohort to re-challenge with EpCAM-negative Panc02 tumors (Fig6A) and evaluated the endogenous immune response *ex vivo* using CD8$^+$ T cells from CR (Fig6E) as

well as with 10X single-cell RNA and TCR sequencing (scRNA-seq, scTCR-seq). To assess whether anti-Panc02 tumor immune protection could be transferred to WT mice bearing Panc02-EpCAM negative tumors, we performed an ACT using *Nr2f6*-modified CAR-T cell-treated CR splenocytes. The results demonstrated that these splenocytes were capable of effectively controlling tumor growth and exhibited a survival benefit when directly compared to animals treated with splenocytes from Panc02 antigen-naïve tumor-bearing mice (Fig6D). An *ex vivo* recall assay demonstrated that endogenous polyclonal $CD8^+$ T cells from *Nr2f6*-modified CR exhibited heightened IFNγ production compared to those from Panc02 tumor antigen-naïve tumor-bearing mice when re-stimulated with tumor cells *ex vivo* (Fig6E). The combined data set provides evidence of a long-lasting CAR-targeted EpCAM antigen-independent immune response accompanied by a transferrable superior tumor rejection phenotype in antigen-naïve tumor-bearing mice when using solely splenocytes isolated from *Nr2f6*$^{crispr-/-}$ CAR-T-treated CR mice. It is therefore evident that the augmented effector functions of *Nr2f6*-modified CAR-T cells play a central role in the initial control of tumors. After this initial phase, the role of ES becomes pivotal in sustaining durable endogenous immunity and preventing tumor relapse.

Integrated remodeling of the tumor–immune landscape by *Nr2f6*-edited CAR-T therapy

To mechanistically understand architectural changes of TILs in the *Nr2f6*-modified CAR-T cell treated CR cohort, we analyzed scRNA- and paired α/β scTCR-seq data obtained from $CD45^+$ TILs on d305 after initial tumor injection and CAR-T cell application (Fig6A). We identified several clusters representing prominent immune cell subtypes (Fig7A) based on their characteristic expression profiles (Suppl.Table2). Strikingly, we observed a marked difference in cell composition between *Nr2f6*-modified CAR-T cell treated CR and Panc02 tumor antigen-naïve mice. *Nr2f6*-modified CAR-T cell-treated CR had reduced numbers of exhausted $CD8^+$ and regulatory T cells and showed, among other changes, an increase in proliferating $CD8^+$ T cells and cDC1s (Fig7B). It is noteworthy that, in the *Nr2f6*-modified CAR-T cell-treated CR cohort, no CAR^+ T cells were detected among TILs, thereby firmly excluding their residual contribution to tumor clearance. Consistent with our working hypothesis, GO analysis of DEGs revealed pathway changes in both proliferating $CD8^+$ T cells (Fig7C) and cDC1s (Fig7D). $CD8^+$ proliferating T cells exhibited an enrichment of pathways linked to positive regulation of T cell differentiation, IL-2 and type II interferon production as well as activation of αβ T cells (Fig7C). cDC1s showed

overrepresentation of terms associated with T cell cytokine production, activation, and differentiation as well as response to type II interferon (Fig7D). To further validate whether ES had occurred, we determined TCR clonality and diversity by scTCRseq. Compared to Panc02 tumor antigen-naïve mice, *Nr2f6*-modified CR showed a decrease in clonality with a concomitant increase in diversity, indicating that T cells were primed against various epitopes without a few being prominent (Fig7E). This pattern was not observed during the initial CAR-T treatment phase; however, enrichment of $CD3^+$ T cells following *Nr2f6*-edited CAR-T therapy (Suppl.Fig8A-C) supports progressive enhancement of endogenous immunity over time, consistent with recent reports[39], and underscores that broadening and adaptation of the endogenous TCR repertoire are predominantly manifested during the memory phase after CAR-T therapy rather than during immediate effector phase.

Safety and translational implications

Although EpCAM is expressed on normal tissue, no evident immune-related adverse effects were observed in mice treated with *Nr2f6*$^{crispr-/-}$ αEpCAM CAR-T cells. Treated animals showed stable weight and serum cytokine levels comparable to controls (Suppl. Fig1A–C). These data indicate an absence of detectable acute toxicity and suggest a favourable short-term safety profile. Importantly, non-lymphodepleting treatment retained efficacy, implying that *Nr2f6* deletion may enhance CAR-T cell activity without increasing immune toxicity. Together, these findings provide a preliminary basis for further evaluation of NR2F6 as a potentially safe intracellular target for augmenting CAR-T therapy in solid tumor models (see schematic cartoon in Fig7F-H).

Discussion

The intrinsic dysfunction of endogenous immune cells within an immunosuppressive TME, combined with high intra-tumor heterogeneity and antigen loss-mediated immune escape, represent pivotal factors in both tumor escape from immune surveillance and resistance to conventional CAR-T therapies [40]. The effective induction of epitope spreading (ES) by CAR-T cells with robustly revived cytotoxic activity potentially addresses these challenges and may help counteract immune suppression within the TME and overcome tumor escape driven by antigen loss and heterogeneity. Previous studies have shown that combining vaccination with CAR-T therapy can enhance endogenous T cell responses [12]. Additionally, recent publications from 2025 underscore a rapidly growing consensus that driving secondary, host-mediated, antigen-agnostic immune control is a critical frontier for advancing CAR-T therapy against heterogeneous solid tumors, thereby directly validating our mechanistic strategy. For instance, armored CAR-T cells engineered to express cytokines such as IL-7, CCL19, IL-12, or IL-18 have demonstrated enhanced recruitment and activation of dendritic cells and endogenous T cells, promoting epitope spreading [41, 42]. Similarly, chemokine-secreting CAR-T cells, such as XCL1, have been shown to recruit cDC1s and boost endogenous $CD8^+$ T cell responses [41]. Besides the mentioned studies, the role of ES during T cell-based therapies remains largely unexamined. This is primarily due to the prevalent practice of lymphodepletion prior to therapy (in both patients and mice), the utilization of immunodeficient mice, and the employment of humanized mice, which lack the host's functional innate and adaptive immune systems. In a distinct and unprecedented advance over these multi-component engineering approaches, our study is the first to show that targeted NR2F6 gene editing in CAR-T cells alone; without additional cytokine expression, vaccination, or combinatorial manipulations, is sufficient to robustly and reproducibly drive polyclonal host immunity and effective immune control of antigenically heterogenous solid tumors *in vivo*. This streamlined, single-gene editing strategy not only establishes a new mechanism, distinct from current approaches, but also highlights an innovative and clinically actionable path toward future CAR-T therapies with enhanced efficacy for solid tumor treatment.

The present study provides compelling evidence that genetically engineered CAR-T cells deficient in the NR2F6 immune checkpoint elicit a robust secondary immune response by the host against

non-CAR-targeted tumor antigens. This effect is due to the significantly restored cytotoxic capacity, cytokine production and metabolic fitness of *Nr2f6*-modified CAR-T cells, which ultimately leads to a deviation of terminal differentiation towards a predominance of Tpex cells over Ttex cells during chronic stimulation. Typically, chronic stimulation induces hypo-responsive exhausted T cells. Exhaustion has been extensively studied in the context of chronic viral infections as well as cancer and is recognized as a hallmark of immunotherapy dysfunction [43, 44, 45]. Tpex, known for their self-renewal potential and expression of TCF1, have been identified as major responders to immune checkpoint blockade and are responsible for therapeutic success highlighting their pivotal role in immunotherapy [46, 47, 48]. Failure of immunotherapy is frequently associated with metabolic dysfunction of the therapeutic agent. Modulation of mitochondrial fitness and OXPHOS has emerged as a promising strategy to boost CAR-T cell functionality and persistence. Consistently, mitochondrial dysfunction occurs as an early event after activation and was reported to be a major driver of T cell exhaustion in the TME [49, 50, 51]. In line with a study showing that increased OXPHOS supports the self-renewal potential of Tpex cells [52], we demonstrate that *Nr2f6*-deficient CAR-T cells maintain their metabolic fitness, as evidenced by robust glycolysis and OXPHOS activity, during chronic stimulation accompanied by an increased proportion of Tpex-like cells with increased TCF1 protein expression underpinning the superior sustained cytotoxic effector functions.

It is noteworthy that in this pre-clinical Panc02-EpCAM model, treatment with *Nr2f6*-modified CAR-T cells resulted in complete remissions in 55% of the treated mice (compared to 10% for NTC CAR-T therapy) in a mouse model of solid tumors. These results were comparable to those obtained with two independent CAR-T mouse models (B16-F10-hEGFR, MC38-hEGFR) (Suppl.Fig2A-G), which demonstrate the broad applicability of the obtained results. NR2F6 exerts immunoregulatory control in both $CD4^+$ and $CD8^+$ T cells, but our data indicate that the enhanced antitumor activity is primarily mediated by $CD8^+$ CAR-T cells (Suppl.Fig2H–K). The observed ES effect likewise depends mainly on *Nr2f6*-modified CAR-T cells, as untransduced bystander T cells failed to confer this benefit (Suppl.Fig4C). Still, we cannot fully exclude minor supportive contributions from endogenous, non-modified T cells that may be secondarily activated following CAR-T-mediated tumor recognition.

Sustained tumor rejection in the Panc02-EpCAM model could not be attributed to the CAR-T cells as they were no longer detectable from day thirteen post-ACT. From a mechanistic standpoint,

through the crucial process of exposing in particular non-self tumor antigens to robust cross-priming, *Nr2f6*-modified CAR-T therapy thus has the potential to promote secondary T cell-based tumor rejection by an intact endogenous immune system in immunocompetent wild type mice. This has the advantageous effect of enabling the endogenous immune system to induce a polyclonal T cell response against multiple tumor antigens. This results in durable and effective anti-tumor immune memory control, even against CAR-targeted antigen-negative tumors, common in antigen-heterogeneous solid tumors. Indeed, *Nr2f6*-modified CAR-T complete responders show identical clearance of CAR-targeted antigen-positive and antigen-negative tumor loads when re-exposed to the tumor six months after initial therapy (Fig6), providing conclusive evidence that this secondary immune response by the host is CAR-targeted antigen-independent. Importantly, we observed no toxicity or on-target/off-tumor effects, underscoring that the use of *Nr2f6*-modified CAR-T cells without lymphodepletion represents a promising strategy with minimal adverse effects while preserving potent endogenous antitumor immunity.

Although model-dependent differences are possible, previous studies have consistently identified NR2F6 as a repressor of effector cytokine transcription across multiple tumor systems [21, 24, 26]. Building on this established checkpoint function, the present work extends NR2F6 biology to the context of engineered adoptive T cell therapy and demonstrates that acute intrinsic editing of NR2F6 within CAR-T cells can potentiate host immunity to achieve durable tumor control in immunocompetent models. As previously reported, immune-deserted tumors, which are associated with poor survival, can be converted into immune-inflamed tumors through ICD, ultimately improving patient outcome [53, 54]. Consistent with this, we demonstrate that *Nr2f6*-modified CAR-T cell therapy primes the endogenous immune system *in vivo*, leading to increased numbers of cDC1s and subsequent recognition of both CAR-targeted and non-CAR-targeted Panc02 tumor antigens by endogenous T cells. The treated cohort exhibited a durable secondary memory response upon re-challenge with CAR-targeted antigen-negative tumors, characterized by reduced exhausted $CD8^+$ T cells and increased proliferating $CD8^+$ T cells and increased active cDC1s, even 300 days after initial therapy. While our data highlight the pivotal role of cDC1s in this process, we cannot exclude possible contributions from other antigen-presenting cell subsets, including monocyte-derived dendritic cells, macrophages, and B cells, which warrant further investigation in future studies. Mechanistically, epitope spreading is likely orchestrated through multiple complementary pathways: enhanced IFNγ secretion by *Nr2f6*-deficient CAR-T cells amplifies

cDC1 activation; loss of NR2F6 lowers the activation threshold of CAR-T cells, inducing a hyper-functional state that strengthens and prolongs direct cytotoxic responses; and immunogenic cell death (ICD) triggered by these effector cells broadens the tumor antigen repertoire, thereby enhancing cross-priming and diversifying host T cell responses. Together, these processes generate robust polyclonal T cell responses against non-CAR targets, potentially forming a self-amplifying circuit of tumor recognition that engages both innate and adaptive immunity. This emphasizes the critical role of an intact host immune system for sustainable tumor control and highlights the potential drawbacks of current lymphodepletion practices in CAR-T patients, which may counteract secondary immune responses.

This study identifies NR2F6 as a T-cell-intrinsic metabolic checkpoint that limits CAR-T cell function in solid tumors. Deletion of *Nr2f6* enhances exhaustion resilience and sustains antitumor activity by coupling cytotoxic reinvigoration with dendritic cell-dependent cross-priming and epitope spreading (ES). These preclinical findings provide a rationale for targeting NR2F6 to overcome immunosuppression and antigenic heterogeneity in solid tumors, with potential relevance for improving CAR-T and other cell-based immunotherapies in human cancer.

Methods

Animals

Male and female C57BL/6N (purchased from Charles River; RRID:IMSR_CRL:027) , B6(C)-Gt(ROSA)26Sorem1.1(CAG-cas9*,-EGFP)Rsky/J (purchased from Jackson; RRID:IMSR_JAX:028555), Pep Boy (B6.SJL-Ptprc^{a} Pepc^{b}/BoyJ, B6 CD45.1, Ly5.1) (purchased from Jackson; RRID:IMSR_JAX:002014), *Rag1*$^{-/-}$ (B6.129S7-Rag1tm1Mom/J; purchased from Jackson; RRID:IMSR_JAX:002216), and *Nr2f6*$^{-/-}$ (described previously in [55]) mice were housed under specific pathogen-free (SPF) conditions, light/dark cycle (12/12), 21-23°C ambient room temperature with 45% humidity, and the mice had ad libitum access to water and food. Animals were controlled frequently by the staff of the animal facility and us. All animal experimentation was performed according to European guidelines and approved by the Austrian federal ministry of education, science and research (2023-0.203.973). When necessary, mice were euthanized using carbon dioxide (CO_2) and cervical dislocation.

Cell lines

The 3-methylcholanthrene-induced mouse pancreatic ductal adenocarcinoma cell line Panc02 (RRID: CVCL_D627) was stably transduced to express murine EpCAM and was a kind gift of Prof. Kobold (LMU, Munich) and has been previously described [56, 57]. Panc02-EpCAM negative tumor cells were enriched using flow sorting. Panc02-EpCAM cells expressing the fluorescent protein GFP were generated by retroviral transduction using the pMP71-GFP construct [58]. GFP^{+} Panc02-EpCAM cells were enriched using flow sorting. B16-F10-hEGFR and MC38-hEGFR were generated in-house by lentiviral transduction using the PWPXLD-EGFR-WT construct (kind gift of Chay Kuo, Addgene, #133749). Mouse tumor cell lines were maintained in DMEM + 10% fetal calf serum (FCS) + 2mM L-Glutamine (L-Glut) + 100U/mL penicillin + 100mg/ml streptomycin, further referred to as DMEM+++, The PlatinumE (PlatE) cells were obtained from Cell Biolabs, Inc. (RV-101; RRID: CVCL_B488) and were tested negative for mycoplasma (Invivogen, rep-mys-20). They were cultured in DMEM+++, supplemented with 1 µg/mL puromycin (Merck, P8833) and 10 µg/mL blasticidin (Sigma, 15205), to ensure transgene expression. This medium is referred to as PlatE medium. All cell lines were cultured in T175 tissue culture flasks (Sarstedt, 833912002), passaged every two days, and routinely tested for mycoplasma, with negative results.

Cell line passaging and harvest

Adherent cell lines were passaged as follows: cell culture vessel, typically a T175 tissue culture flask (Sarstedt, 833912002), was washed once with 6mL warm 1x phosphate buffer saline (PBS) and then dissociated using 3mL TrypLE Express (Thermofisher, 12604021)for a few minutes at 37°Cuntil cells started to float. Reaction was stopped by adding twice the amount of cell culture medium. Cell suspension was transferred to a Falcon tube and centrifuged at 300 × g/rcf for 5 minutes at room temperature (RT). Cells were then used for *in vitro* assays, *in vivo* experiments or resuspended in 1mL cell culture medium and split accordingly: tumor cells typically 1:10 and PlatE 1:5 depending on application.

Primary mouse T cell isolation

Primary mouse T cells were isolated by negative selection using primarily the $CD8a^+$ T cell isolation kit (Miltenyi, 130-104-075) or once the untouched CD4 isolation kit (Miltenyi, 130-104-454). In brief, mice were euthanized and spleen as well as lymph nodes were excised. After pressing organs through a sieve to achieve a single cell suspension, cells were resuspended in 3mL red blood cell (RBC) lysis buffer (0.15M NH_4Cl, 10mM $KHCO_3$, 0.1mM ethylenediaminetetraacetic [EDTA] dehydrate in ddH_2O) per spleen and incubated for 5min at RT. Reaction was stopped by adding twice the amount of buffer C (PBS supplemented with 0.5% bovine serum albumin [BSA] and 2mM EDTA). Splenocytes were counted and incubated with biotinylated antibodies and magnetic beads according to manufacturer's instructions. $CD8^+$ or $CD4^+$ T cells were enriched by applying the cell suspension on LS columns (Miltenyi, 130-042-401) placed onto a strong magnet. Columns were flushed twice with 3mL of buffer C and flow through was collected. Enriched T cells were then counted with LUNA automated cell counter (Logos Biosystems) and used for downstream applications. Enriched T cells were checked for purity using FACS analysis.

Plasmids and constructs

For retroviral production, the pMP71 and MSCV backbones (provided by C.Baum, Hannover or purchased from Vectorbuilder) were used for transfections. The second-generation chimeric antigen receptor (CAR) targeting murine EpCAM on the pMP71 backbone was previously

described [56, 57]. The CAR targeting human EGFR on a MSCV backbone was purchased from Vectorbuilder. Briefly, the CARs consist of a single-chain variable fragment (scFv) (EpCAM: clone G8.8, EGFR: Cetubixmab) fused to a CD8 hinge and a CD28 transmembrane region. Intracellularly, they consist of a CD28 co- (UniProt entry P31041; amino acids 151–218) and a CD3zeta stimulatory domain (UniProt entry P24161; amino acids 52–164). CAR detection was either possible by a myc-tag between the scFv and the hinge region or by GFP expression, which was separated from the CAR by a P2A self-cleavage sequence. The pMP71-GFP plasmid [58] was used as a control and to transduce tumor cell lines. The PWPXLD-EGFR-WT was a gift from Chay Kuo (Addgene plasmid # 133749,RRID:Addgene_133749) and was used to transduce the melanoma tumor cell line B16-F10 and the colorectal cancer cell line MC-38. All plasmids were visualized on https://benchling.com.

Transfection of PlatE cells and virus production

For optimal viral production, PlatE cells were split three times a week and cultured not more than 12 weeks after thawing as recommended by the supplier. The day prior to transfection, 8×10^5 PlatE cells were seeded into tissue culture-treated 6-well plates (Szabo Scandic, 35 3046) in PlatE medium and incubated overnight at 37°C and 5% CO_2 to reach a confluency of around 70%. On the day of transfection, PlatE medium was discarded and 3mL DMEM supplemented with 10% FCS and 2mM L-Glut without antibiotics was added. Transfection was carried out using the calcium precipitation method: per well, 15µL calcium chloride (2.5M) was mixed with 18µg of transfer plasmid (pMP71-CAR or pMP71-CAR-GFP) and ddH_20 to a final volume of 150µL. This was slowly added into 150µL transfection buffer (1.6g NaCl (Merck, 1064041000), 74mg KCl (VWR, 1049361000), 50mg Na_2HPO_4 (Sigma Aldrich, 255793), 1g HEPES (Sigma Aldrich, H0887), in 100mL H_2O, pH 7.1) in a dropwise manner while vortexing constantly. The mix was incubated for 30min at RT. 300µL of the transfection mix was then added onto PlatE cells and incubated for 6 hours at 37°C 5% CO_2. After incubation, medium was discarded and 3mL DMEM+++ were added and plates were put at 37°C 5% CO_2 for 42 hours.

T cell activation and culturing for CAR transduction

12-well plates (Fisher Scientific, 150628) were incubated with 5µg/mL αCD3 antibody (BioXCell, CP082) solution overnight at 4°C. After negative selection on day 0, CD8 or CD4 T cells were

resuspended at 3 × 10^6/mL in CAR RPMI (RPMI 1640 + 10% FCS + 100U/mL penicillin + 100mg/ml streptomycin (M&B Sticker, P06-07100) + 2mM L-Glutamine (M&B Sticker, P04-80050) + 1mM sodium pyruvate (Sigma Aldrich, S8636) + 1mM HEPES (Sigma Aldrich, H0887) + 50µM 2-mercaptoethanol (Sigma Aldrich, M3148)). Coated plates were washed twice with 1x PBS before seeding 3 × 10^6 T cells into pre-coated wells. Medium was supplemented with 1µg/mL αCD28 antibody (BioXCell, CP042) and 10ng/mL IL-2 (Biolegend, 589106). Plates were incubated overnight at 37°C and 5% CO_2.

Retroviral transduction of T cells and CAR detection

In general, CAR-T cells used for *in vivo* experiments were transduced with a CAR together with a GFP reporter, whereas CAR-T cells for *in vitro* experiments were transduced with a CAR only. For viral transduction, non-tissue culture-treated 24-well plates (Corning, 351147) were coated with 12.5µg/mL Retronection solution (Takara, T100B) overnight at 4°C. The next day, plates were blocked with ddH_2O supplemented with 2% BSA fraction V (Roth, T844.2) for 30min at 37°C. In the meanwhile, supernatant containing CAR viral particles was harvested from PlatE cells and filtered through a 0.45µm cellulose-acetate syringe filter (Integra Biosciences, 158015). 2mL fresh DMEM+++ was added to PlatE cells to harvest supernatant again after 24 hours. After blocking, plates were washed with 1x PBS supplemented with 25mM HEPES and finally 2mL of viral supernatant was added to each well of the Retronectin-coated plate and spun at 3000 × g for 2 hours at 4°C. One hour before the end of the spin, T cells were prepared. Approximately 22 hours after plate-bound activation, T cells were harvested and counted using a LUNA automated cell counter. T cells were adjusted to 1 × 10^6/mL in CAR RPMI supplemented with 10ng/mL hIL-2 and mouse αCD3/CD28 activation beads (Thermo Fisher, 11453D) at a ratio of one bead per T cell (25µl bead solution/mL). After the spin, viral supernatant was discarded, and 1mL T cell suspension was added per well. Plates were spun at 800 × g for 30min at 32°C in a table-top centrifuge and put at 37°C 5% CO_2 overnight. The next day, viral supernatant was harvested again from PlatE cells and filtered through a 0.45µm cellulose-acetate syringe filter (Integra Biosciences, 158015). 0.5mL of the viral particle containing supernatant was mixed with 0.5mL CAR RPMI and 1mL of the mix was added directly to T cells. Plates were then spun a second time at 800 × g for 30min at 32°C and incubated for another 5 hours. After this last incubation, T cells were harvested, activation beads were removed, and T cells were counted. Cells were then adjusted to

1.5 × 10^6/mL in CAR RPMI supplemented with 10ng/mL interleukin 15 (IL-15, Biolegend, 566302) as well as interleukin 7 (IL-7, Biolegend, 577804) and seeded into 24- or 12-well plates. Cultures were maintained at 1.5 × 10^6/mL in IL-15 and IL-7 containing medium. Transduction efficiency of αEpCAM CAR was assessed either by using a αc-myc FITC antibody (Miltenyi; clone: REA1287, 130-116-485) or GFP by flow cytometry. For detection of αEGFR CARs, T cells were stained with recombinant biotinylated EGFR (Creative Biolabs, CARD-LX025) and Streptavidin coupled to bv421 (Biolegend, clone 3A20.2 405226). For *in vitro* experiments CAR-T were used on the 5th day after isolation, whereas for *in vivo* experiments CAR-Ts from the 7th day were used.

Genome editing of CAR-T cells using CRISPR/Cas9

For acute depletion of *Nr2f6* in $CD8^+$ and $CD4^+$ (CAR) T cells, the CRISPR/Cas9 system was applied. In this case, (CAR) T cells from Cas9 transgenic mice were electroporated with synthetic *Nr2f6* targeting guide (g)RNAs (Horizon Discovery, see below and Suppl.Table4) 48 hours after T cell activation using the Amaxa mouse T cell nucleofactor kit (Lonza, VVPA-1006) on the nucleofector 2b device (Lonza Biosciences). In this study, different kinds of guides with different targeting sites in the *Nr2f6* gene were used. sgRNA.3 (sg03) was used directly, whereas crispr (cr)RNA.4 (crRNA.4) and the non-targeting control (NTC) crRNA were annealed with a corresponding tracr RNA to yield a fully competent gRNA. Therefore, 200µM crRNA and 200µM tracrRNA solution in a ratio of 1:1 were heated to 95°C in a thermocycler and left to cool at RT to allow sufficient complexing. Five hours after the second spin transduction, transduced T cells were harvested and counted. 1 × 10^7 T cells were pelleted and transfected with 3.1µM *Nr2f6* or NTC gRNA solution. T cells were electroporated using the X-001 program on a Nucleofector 2b device (Lonza) and immediately recovered in transfection medium supplemented with 10% FCS, 2mM L-Glut, 100IU/mL Pen/Strep and medium component A and B in a 12-well plate according to manufacturer's protocol. After a 1-hour rest, 1mL CAR RPMI containing 20ng/mL IL-7 (Biolegend, 577804) and IL-15 (Biolegend, 566302) was added per 1mL T cells. T cells were passaged the next day. Gene editing efficiency was analyzed using the Tracking of Indels by Decomposition (TIDE) algorithm [59]. *Nr2f6*-crRNA.4 (CM-045088-04-0010; 5' CTCAAGAAGTGCTTCCGGGT 3'); *Nr2f6*-gRNA.3 (SG-045088-03-0010; 5'

CCGCAATCTCAGCTACACCT 3'), NTC-gRNA (U-007501-01-20), tracrRNA (U-002005-50). See also Suppl.Table4.

Tumor inoculation and ACT with gene-edited CAR-T cells

Panc02-EpCAM, B16-F10-hEGFR or MC38-hEGFR were cultured as described above and were checked for EpCAM or EGFR expression by flow cytometry prior to injection. The day before, tumor cells were split 1:2 to ensure ~70% confluency on day of injection for sufficient engraftment *in vivo*. Mice used for *in vivo* experiments were shaved a few days before the injection of tumor cells to mitigate stress. For Panc02-EpCAM experiments, 1×10^6 syngeneic tumor cells were injected subcutaneously (s.c) into the right flank of 8- to 12-week-old immunocompetent female mice. Both homogenous, e.g. 100% EpCAM positive or 100% EpCAM negative, and heterogeneous, e.g. 70% EpCAM positive + 30% EpCAM negative, tumor loads were used, respectively. For B16-F10-hEGFR and MC-38-hEGFR experiments, 1×10^6 (B16-F10-hEGFR) or 5×10^5 (MC-38-hEGFR) tumor cells were injected subcutaneously (s.c) into the right flank of 8- to 12-week-old immunocompetent female wild-type mice (Charles River, 027C57BL/6). Two days (Panc02-EpCAM) or 5 days (B16-F10-hEGFR, MC38-hEGFR) later when tumors reached an approximate size of 50 mm^3, tumor bearing mice were randomly assigned into different treatment groups based on their tumor size and injected intravenously (i.v.) with 3.6×10^6 (Panc02-EpCAM and MC-38-hEGFR) or 1×10^6 (B16-F10-hEGFR) NTC or *Nr2f6* CRISPR/Cas9 gene-edited $CD8^+$ CAR-T cells in 50µL PBS (used for almost all experiments), or 4×10^6 *Nr2f6* CRISPR/Cas9 gene-edited $CD8^+$ + $CD4^+$ CAR-T cells (Suppl.Fig2H-K). As a control, *NTC* as well as *Nr2f6*-depleted polyclonal $CD8^+$ T cells were injected i.v. into Panc02-EpCAM tumor bearing mice. Tumor growth and mouse weight were assessed three times per week using a digital caliper and a scale, respectively, and tumor size was calculated with the following equation: $V = {}^1/_2\, x\ (length\ x\ width^2)$. Tumor measurement was performed in a double-blinded fashion. Mice were euthanized using CO_2 and cervical dislocation when tumors reached 1500mm^3, a 20 percent weight loss was observed or when animals were multimorbid. For survival analysis, data were collected in Kaplan-Meier plots. For experiments using immunodeficient *Rag1*$^{-/-}$ mice, animals were inoculated with 5×10^5 Panc02-EpCAM cells and treated with 1×10^6 gene-edited $CD8^+$ CAR-T cells on day two after tumor injection.

Detection of CAR-T cells and analysis of innate immune cells in tumor bearing mice using multicolor flow cytometry

Ly5.1 recipient mice were challenged with Panc02-EpCAM tumors and treated with *NTC or Nr2f6* gene-edited CAR-T cells two or three days later as stated above. For CAR-T cell detection over time, blood was collected from tumor-bearing mice using a lancet and an EDTA (Sigma Aldrich, 03690) containing tube on day 6 and 13 after tumor injection. Red blood cell (RBC) lysis was performed using 40µL blood and in-house Erylysis buffer (described above). Cells were washed thoroughly with buffer C before FcR-block (BD Biosciences; Clone 2.4G2, 553142) was added to prevent unspecific binding. Cells were then stained for viability using fixable viability stain (FVS)780 (BD Biosciences; 565388; 1:2000) and the following surface antibodies: CD45.1 Pacific blue (Biolegend; clone: A20, 110721), CD45.2 PE (Biolegend; clone: 104, 109807), CD4 V500 (BD Biosciences; clone: RM4-5, 560782), CD8 APC (Biolegend; clone: 53-6.7, 100712), CD3 PE-Cy7 (eBiosciences; clone: 17A2, 25-0032-82). Samples were run on a BD FACS Canto II on medium flow rate. CAR-T cells were identified by CD45.1- $CD45.2^+$ GFP^+ staining in the FlowJo software (v10.9.0).

For analysis of the innate immune cell compartment, we used a multicolor FACS panels. Therefore, mice were euthanized as indicated in the figure legends. Spleens were harvested and meshed through a sieve to yield a single cell suspension. After RBC lysis, splenocytes were counted, 2×10^6 were transferred to a 96-well round bottom plate (Szabo Scandic, 35 3077) and first stained for viability using FVS440UV according to manufacturer's instructions (1:1000; BD Biosciences; 566332). Next, FcR-block (BD Biosciences; Clone 2.4G2, 553142) was added followed by the antibody mix (Suppl.Table3) in a total volume of 50µL. Of note, brilliant stain buffer (1:10; BD Biosciences, 566349) was added to the antibody mix to prevent clogging of brilliant dyes. After 20min of incubation, cells were washed twice and acquired on a Cytek Aurora machine (5 laser configuration). Unmixing was performed using a mix of cell and bead samples, respectively, and checked using single stains. Populations were verified using fluorescence minus one (FMO) controls. Data was analyzed in FlowJo (v10.9.0).

ELISpot

Immunocompetent $Ly5.1^+$ recipient mice were injected with 1×10^6 Panc02-EpCAM tumor cells and treated with 3.6×10^6 $CD45.2^+$ CAR^+ T cells two days later. On day 21 after tumor injection,

mice were euthanized, spleens were harvested and pressed through a sieve to yield a single cell suspension. After RBC lysis, splenocytes were counted and CD45.2$^+$ CAR-T cells were depleted using a biotinylated CD45.2 antibody (Miltenyi; clone: REA1223, 130-124-089). Subsequently CD3$^+$ T cells were negatively isolated using the pan T cell isolation kit (Miltenyi, 130-095-130) according to manufacturer's recommendations and subjected to ELISpot assay.

For antigen presentation, mouse bone-marrow-derived dendritic cells (BMDCs) were generated as described elsewhere [60] and either left unstimulated or stimulated with an activating antibody against CD3 (Mabtech, Nacka Strand, Sweden, 3605-1-50) as positive control as well as a set of peptides and lysates. For peptide stimulations, dendritic cells were loaded with a pool of control peptides (peptide control) consisting of mouse-unspecific CEF/CEFTA as well as SARS-CoV-2 spike peptide pools (Miltenyi Biotec, Bergisch Gladbach, Germany). Additionally, tumor specific peptides were combined into two different peptide pools (Peptide pool 1 and Peptide pool 3). Lyophilized peptides were reconstituted in DMSO at a stock concentration of 10 mg/ml and used at a final concentration of 2 µg per 100 µL. Similarly, dendritic cells were loaded with lysates from the human monocytic cell line THP-1 as a control (Lysate control), as well as with lysates from the tumor cell line both before (Cell lysate) and after (Tumor lysate) injection and growth within the mice at a 1:10 dilution. Peptide and Lysate loading was performed in culture medium (RPMI with 10% FBS, 1% L-glutamine, 1% penicillin/streptomycin; all reagents obtained from Sigma Aldrich, St. Louis, MO, USA) for 2h at 37°C and 5% CO_2. To detect activated and specific T cells, we used a Mouse Granzyme B ELISpot Kit (EL1865, BioTechne, Minneapolis, MN, USA). The precoated plates were initially washed three times with sterile-filtered 1x PBS and blocked for 30 minutes using CAR RPMI. During this time, the previously loaded or unstimulated BMDCs (2×10^4 cells per well) were washed three times with 1x PBS to remove excess peptides or lysate and combined for antigen presentation with the rested CD3$^+$ T cells (2×10^5 cells per well). The cell suspensions were then transferred onto the respective ELISpot plates and incubated over night at 37°C and 5% CO_2. Further detection and development were performed according to the manufacturer's instructions. In brief, cells were discarded and plates washed five times with sterile-filtered PBS or the designated wash buffer. After the last wash, detection antibody was added and plates incubated for 2h at room temperature. Detection solution was discarded, and plates washed again five times as described above. Next, Streptavidin-AP (Granzyme B kit) was added, and plates incubated in the dark for 1h at room temperature. Following another set of

washes, the Granzyme B plates were incubated with BCIP/NBT substrate (BioTechne, SEL002) for 1h and then washed thoroughly with tap water. All plates were left to dry before further analysis. Imaging, counting and quality control of ELISpot plates were performed using the Immunospot Analyzer S6 Ultra M2 (CTL, Cleveland, OH, USA).

Tumor re-challenge of relapse-free complete responder mice

Prior to re-challenge, tumor cells were enriched for EpCAM positive and EpCAM negative cells using flow sorting and maintained in DMEM+++. Six months after first tumor challenge, mice, which showed complete response (CR) after treatment with *NTC* and *Nr2f6* acute gene-edited CAR-T cells, were injected with 2.5×10^6 EpCAM positive and 1×10^6 EpCAM negative Panc02 tumor cells into the right and left flank, respectively. Panc02-naïve female C57BL/6 mice were used as controls and injected with an identical tumor load. Monitoring of tumor-bearing mice was performed as described above.

Immune memory transfer from complete responders to CAR-antigen naïve mice, *ex vivo* recall assay and cell preparation for scRNAseq

Relapse-free complete responder (CR) mice, which survived the 1st re-challenge, were injected again with 1×10^6 Panc02-EpCAM negative tumors. Panc02 antigen-naïve C57BL/6 mice were used as controls and injected with the same tumor load. Five days later, mice were euthanized and spleens and tumors were harvested. Single cell suspensions of spleens were prepared as described above. 1×10^7 splenocytes from CR or antigen-naïve mice were transferred into Panc02-EpCAM negative tumor-bearing mice 2 days after tumor initiation. Tumor growth and survival were assessed, and mice were euthanized if abort criterion were met. Remaining splenocytes were subjected to CD8 T cell isolation using the untouched $CD8a^+$ T cell isolation kit (Miltenyi, 130-104-075). Enriched CD8 T cells from CR and antigen-naïve mice were then co-cultured with Panc02-EpCAM in an E:T ratio of 5:1 for 24 hours at 37°C and 5% CO_2. The next day, Golgi Plug and Stop (1:1000 [555029] and 1:1500 [554724]; BD Bioscience) were added and incubated for 5 hours. After incubation T cells were harvested and subjected to intracellular FACS analysis.

For scRNA-seq, tumors were digested in DMEM+++ supplemented with Liberase TL (Merck, 5401020001, 10mg/mL) and DNAse I (Roche, 11284932001, 20mg/mL) for 30min at 37°C 5% CO_2. 0.5M EDTA (Sigma Aldrich, 03690) was added for 5min before meshing tumors through a

20µm cell strainer (Corning, 156499). Tumor single cell suspensions were stained using CD45 PE (Thermo Fisher, clone: I3/2.3, 12045183) for 20min at 4°C. $CD45^+$ leukocytes were flow sorted at the FACS Core Facility of the Medical University of Innsbruck. Library preparation and scRNA-seq was performed by the MulitOmics Core Facility of the Medical University of Innsbruck.

Single-cell sequencing

Single-cell suspensions were processed at the Medical University of Innsbruck MultiOmics Sequencing Core Facility. Adequate Cell viability and concentration was verified with trypan blue (Biorad, 1450021) staining and TC10 automated cell counting (Biorad) complemented with hemocytometer visual inspection. Final cell suspensions were processed with a Chromium single cell controller (10xGenomics, 1000127) and Chromium Next GEM Single Cell 5' Kit v2 (10xGenomics, 1000269) chemistry, targeting 4000-6000 cells per sample. The resulting total RNA and V(D)J libraries were multiplexed and sequenced with Illumina Hi-Seq technology, generating in total approximately 700 M read pairs.

Retroviral and lentiviral transduction of tumor cell lines

Retrovirus containing supernatant was produced as described above. For Panc02-EpCAM-GFP, PlatE cells were transfected with 18µg of transfer plasmid (pMP71-GFP) to produce viral particles. The day prior transduction, 2×10^5 Panc02-EpCAM were seeded into 6-well plates (Szabo Scandic, 35 3046) and incubated overnight at 37°C and 5% CO_2. The next day, medium was replaced by 2mL DMEM+++ supplemented with 8µg/mL polybrene (Sigma-Aldrich, TR-1003-G). Then 2mL of filtered viral supernatant was added directly and the plates were spun at 800 × g for 2 hours at 32°C. Transduction efficiency was assessed by flow cytometry. GFP^+ cells were enriched by flow sorting. Lentiviral supernatants for B16-F10-hEGFR and MC38-hEGFR production were generated as follows: the day prior to transfection, HEK 293T cells were seeded in 10cm dishes (Thermo Scientific, 353003) at 5×10^6 per dish and incubated overnight at 37°C 5% CO_2. On the next day, medium was replaced with DMEM + 10% FCS + 2mM L-Glutamine and cells were transfected with 5.75µg pHELP1 (PLP1), 5.75µg pHELP2 (PLP2), 3.45µg pHELP3 (VSVG) and 18µg PWPXLD-EGFR-WT (kind gift of Chay Kuo, Addgene, 133749) per dish using Lipofectamine 2000 reagent (Thermo Fisher Scientific, 11668019) according to manufacturer instructions. Supernatant was harvested 48 and 72 hours after transfection and concentrated using the Lenti-X-Concentrator (Takara, 631232) according to manufacturer instructions. Concentrated

virus was pooled and frozen at -80°C. The day prior transduction, 2×10^5 B16-F10 or MC-38 were seeded into 6-well plates (Szabo Scandic, 35 3046) and incubated overnight at 37°C and 5% CO_2. The next day, medium was replaced by 2mL DMEM+++ supplemented with 8µg/mL polybrene (Sigma-Aldrich, TR-1003-G). Then 20µL of concentrated lentiviral supernatant was added directly and the plates were spun at 800 × g for 2 hours at 32°C. Transduction efficiency was assessed by flow cytometry using αEGFR-AF647 (Biolegend, clone AY13, 352917). $EGFR^+$ cells were enriched by flow sorting.

Chronic stimulation assay and live cell imaging

To ensure sufficient target expression, Panc02-EpCAM-GFP^+ were subjected to flow sorting the week prior to the assay. Therefore, tumor cells were stained with αEpCAM-APC (Miltenyi; clone: REA977, 130-123-810) and the EpCAM-high GFP-positive population was sorted directly in DMEM+++ on a FACS Aria (BD Biosciences) machine at the FACS Core facility of the Medical University Innsbruck. Flow sorted tumor cells were cultured at 1×10^6 cells per T175 tissue culture flask (Sarstedt, 833912002). On the first day of the assay, 6×10^4 Panc02-$EpCAM^{hi}$-GFP^+ cells were seeded into 96-well flat bottom plates (Szabo Scandic, 353072) in CAR RPMI and left to adhere for a few hours. After CAR-T production and assessment of transduction efficiency, bulk transduced T cells were counted and adjusted to 3×10^6 CAR^+/mL. 3×10^5 CAR-T cells were then added at an effector:target ratio (E:T) of 5:1 to tumor cells in CAR RPMI without cytokines. Live cell imaging was performed in an Incucyte® live cell analysis system (Sartorius) using the 10x objective. Fluorescence pictures were taken every two hours for up to 10 days. Every 48 hours, co-cultures were taken from the Incucyte machine and CAR-T cells were re-stimulated with fresh target cells. For this, Panc02-$EpCAM^{hi}$-GFP^+ cells were harvested from T175 tissue culture flasks (Sarstedt, 833912002) and resuspended at 6×10^5/mL in CAR RPMI. 100µL of medium was removed from the co-cultures and stored at -20°C for cytokines assessment. Then, 100µL tumor cell suspension was added, and plates were put back into the Incucyte. It was made sure that at least one hour lies between re-stimulation and the next scan to allow sedimentation of tumor cells. Cytotoxicity was determined by decreasing GFP fluorescence and plotted relative to the first scan after each re-stimulation (green integrated intensity per mm^2 relative to first scan after re-stimulation). Analysis was performed using the built-in analysis software (Sartorius). CAR-T cells from single mice in duplicates were considered as biological replicates.

Surface and intracellular antibody staining of mouse CAR-T cells

Staining was performed with up to 1×10^6 (CAR) T cells in a 96-well round bottom plate (Szabo Scandic, 353077). For viability assessment, T cells were washed twice with Hanks buffered salt solution (HBSS) containing Magnesium and Calcium (Pan Biotech, P04-32505). Then, 100µL HBSS supplemented with FVS780 (BD Biosciences, 565388) at a final dilution of 1:2000 was added and incubated for 10 minutes at RT in the dark. After the incubation, cells were washed with buffer C (described above) and subjected to surface antibody staining. Surface antigens were stained for 20 minutes at 4°C in a 40µL reaction in buffer C using the following antibodies: c-myc FITC (Miltenyi, clone: REA1287, 130-116-485), Ly108 Pacific blue (Biolegend, clone: 330-AJ, 134608), PD-1 bv510 (Biolegend, clone: 29F.1A12. 135241), Tim3 PerCp-Cy5.5 (Biolegend, clone: B8.2C12, 134011), Lag3 PE-Cy7 (Biolegend, clone: C9B7W, 125225), CD39 PE (Biolegend, clone: Duha59, 143804), CD45 APC (Fisher Scientific, clone: I3/2.3, 17-0451-82), CD44 PE-Cy7 (Biolegend; clone: IM7, 103030), CD62L APC (BD Biosciences; clone: MEL-14, 553152). For intracellular (IC) cytokine staining, CAR-T cells were transferred to 96-well round bottom plates (Szabo Scandic, 353077) and stained with surface antibodies as stated above. Thereafter cells were fixed using the fixation buffer from Biolegend (420801) for 20 minutes at RT. After fixation, cells were permeabilized by washing twice with the kit's Perm/Wash buffer (1x, Biolegend, 421002). Intracellular proteins were stained for at least 30 minutes to one hour at 4°C in Perm/Wash buffer using the following antibodies: IFNγ PE-Cy7 (Biolegend; clone: XMG1.2, 505826), TNF PerCpCy5.5 (Biolegend; clone: MP6-XT22, 506322), IL-2 APC (BD Biosciences; clone: JES6-5H4, 554429), GZMB PE (Biolegend; clone: QA18A28, 396406). For transcription factor staining, CAR-T cells were chronically stimulated with Panc02-EpCAM^{hi}-GFP^{+}. On day four of co-culture, wells were harvested and transferred to a 96-well round bottom plate (Szabo Scandic, 353077) and stained for surface antigens as described above before fixation using the Foxp3 fixation kit (eBiosciences, 00-5523-00) for 30 minutes at 4°C. Cells were permeabilized twice with 1x Perm/Wash and stained with IC antibodies for one hour at 4°C: TCF1 Pacific blue (Cell Signaling; clone: C63D9, 9066S) and TOX APC (Miltenyi; clone: REA473, 130-118-335). After antibody staining cells were wash twice and resuspended in 200µL buffer C before acquisition on a FACS Canto II (BD Biosciences). For absolute cell counts, precision count beads (Biolegend, 424902) were applied. Therefore, cells were stained directly in culture medium

for 20 minutes at 4°C. Plates were spun and cells were resuspended in 100µL buffer C. 100µL precision count beads were added per sample. Total cell counts were calculated according to the manufacturer's instructions. Data was analyzed using FlowJo software (BD Biosciences, version 10.9.0).

Cytokine production assay

On day 5 of CAR-T production, 6×10^4 Panc02-EpCAM^{hi}-GFP$^+$ cells were seeded into 96-well flat bottom well plates (Szabo Scandic, 353072) and incubated for a few hours to allow attachment. Then, 3×10^5 CAR$^+$ T cells were added (E:T ratio of 5:1) and incubated overnight in CAR RPMI without cytokines. The next day, Golgi Plug and Stop (1:1000 [555029] and 1:1500 [554724]; BD Bioscience) was added for 6 hours before cells were subjected to antibody staining and IC FACS analysis.

Gasdermin E clipping assay

1.5×10^6 CAR-T cells were co-cultured with Panc02-EpCAM^{hi}-GFP$^+$ in a 24-well plate (Szabo Scandic, 35 3047) at an E:T of 5:1. CAR-T cells were re-stimulated every second day with 3×10^5 fresh tumor cells. On day 4, wells were harvested by trypsinization 6 hours after re-stimulation. Briefly, cell culture medium was collected in a 15mL Falcon tube, wells were wash with 1x PBS and 400µL TrypLE Express (Fisher Scientific, 12604013) was added per well. When adherent cells started to detach, 800µL CAR RPMI was added to stop the reaction and medium was transferred to 15mL tube. After a wash step with ice-cold 1x PBS, cells were resuspended in 30µL RIPA buffer (Sigma-Aldrich, R0278) supplemented with 5mM EDTA (Sigma Aldrich, 03690) and 1x Halt protease and phosphatase inhibitor cocktail (ThermoFisher, 78444/10137963) and incubated for 30 minutes on ice while vortexing frequently. Then, lysates were spun for 15 minutes at 15000 × g at 4°C. Supernatant was transferred to a new 1.5mL Eppendorf tube, supplemented with 5µL Pierce Lane Marker Reducing Sample Buffer (Thermo Fisher Scientific, 11809340/39000) and frozen at -80°C. Samples were thawed, heated to 95°C and subjected to immunoblotting using the following antibodies: DFNA5/GSDME (Abcam, clone: EPR19859, ab215191, 1:1000), beta-actin (Santa Cruz; clone: sc-47778, 1:1000). Bands were quantified using ImageJ (v1.51).

Cytokine detection in supernatant

Cytokine release was measured in supernatants using the Luminex xMAP technology. In brief, frozen supernatants were thawed and diluted in CAR RPMI. Assays for IFNγ (Biorad, 171-G5017M) and GZMB (ThermoFisher, EPX010-26074-901/17886521) detection were performed according to manufacturer's instruction on a Bio-Plex 200 machine (Biorad). Absolute concentrations were determined using a standard curve.

Mouse cytokine array

WT mice were treated on d4 after tumor injection (1×10^6 Panc02-EpCam) with 3.5×10^6 NTC or *Nr2f6* acute gene-edited CAR-T cells. On day 3 after CAR ACT mouse spleens were harvested and half a spleen was homogenized in 500µl PBS with cComplete-proteinase inhibitor cocktail, (Fisher Scientific, 78444/10137963) and 1% TritonX100 (Sigma Aldrich, T8787 – 100) on ice. After one freezing step at -70°C lysate was centrifuged at 10.000 rcf for 5 min to remove cellular debris and protein concentration was measured by Bradford assay (BioRad). Protein equivalents (300µg) were used to probe cytokines/chemokines using the Proteome Profiler Mouse Cytokine Array Kit, Panel A (R&D Systems, ARY006) according to the manufacturer´s instructions. Quantification of the spot intensity on the blot membranes was done after background subtraction with QuickSpots software (Ideal Eyes Systems, Inc.).

RNA isolation and qRT-PCR

To assess *Nr2f6* mRNA induction during CAR-T production, $1\text{-}2 \times 10^5$ T cells were harvested, washed once with 1x PBS and resuspended in 350µL RLT buffer (Qiagen, 74106) and stored at -80°C. For co-culture samples, cells were harvested, and live (CAR) T cells were enriched by density gradient centrifugation. Briefly, cells were resuspended in an 80% Percoll solution (Sigma-Aldrich, GE17-0891-01) in HBSS (Thermo Fisher Scientific, 14185052). A 40% Percoll layer was loaded on top, and cells were spun at 250 × g for 30min without a break. After the spin, the interface layer was harvested and subjected to CAR positive selection using αmyc-Biotin (Biolegend; 1µg/mL, 908805) and αBiotin microbeads (Miltenyi; 130-090-485, 20µL for 10^7 cells) according to manufacturer's instructions. $1\text{-}2 \times 10^5$ CAR^+ T cells were then resuspended in 350µL RLT buffer and stored at -80°C.

For quantitative real-time PCR (qRT-PCR), total RNA was isolated using the RNeasy Mini kit (Qiagen) according to manufacturer's instruction and subjected to cDNA synthesis using Omniscript RT kit (Qiagen, 74106) in a 20µL reaction using random hexamer as well as Oligo(dt)-primer (Fisher Scientific, 18418012). qRT-PCR was performed in duplicates using the LUNA mastermix (New England Biolabs, M3004E) and pre-designed *Nr2f6* Taqman primers (Fisher Scientific, see below) on a 7500 Real-Time PCR machine (Applied Biosystems). Target gene expression was normalized to *Rlp13a* (see below) using the ΔΔct method. Ct values over 32 were considered as not expressed. Primers used for qPCR-RT: Mm01340321_m1, Mm01612986_gH.

Seahorse Cell Mito Stress assay

For analysis of oxidative phosphorylation (OXPHOS), 2×10^5 CAR-T cells were seeded into poly-lysine pre-coated Seahorse culture plates in XF RPMI without phenol red (Agilent, 103681) supplemented with 20mM glucose, 2mM glutamine and 1mM pyruvate (all Agilent, 103681-100). Assay was performed using the Cell Mito Stress Test Kit (Agilent, 03010-100) on a Seahorse XFp device (Agilent). Briefly, Seahorse plates were put in a CO_2-free incubator for one hour to allow equilibration. Mitochondrial respiration was analyzed first by assessing the basal respiration, then injecting 1.5µM of the ATP synthase inhibitor oligomycin (Enzo Life Sciences, ALX-380-037-M005), 1µM of the uncoupler carbonyl cyanide-*4*-(trifluoromethoxy)-phenylhydrazone (FCCP, Enzo Life Sciences, BML-CM120-0010) and finally 0.5µM of rotenone/antimycin A (Enzo Life Sciences, ALX-380-075-M010). Results were analyzed using the Seahorse Wave Software (Agilent).

Flow sorting of tumor and CAR-T cells

Panc02-EpCAM, B16-F10-hEGFR, MC-38-hEGFR tumor cells were harvested as described above. Cells were transferred to FACS tubes and up to 1×10^7 cells were stained in 100µL buffer C containing αEpCAM-APC (Miltenyi, clone: REA977, 130-123-810) or αEGFR-AF647 (Biolegend, clone AY13, 352917) antibodies for 20 minutes at 4°C. After incubation, tumor cells were washed twice with buffer C and finally resuspended in ice-cold DMEM+++ supplemented with 2mM EDTA at 1×10^7/mL. CAR-T cells from co-culture were harvested and transferred to a FACS tube for antibody staining. Up to 10^7 cells were resuspended in 100µL buffer C containing αc-myc FITC (Miltenyi, clone: REA1287, 130-116-485), αCD45 APC-Cy7 (Biolegend, clone:

30-F11, 103116) and αEpCAM APC (Miltenyi, clone: REA977, 130-123-810) and incubated for 20 minutes at 4°C. Then, cells were washed twice with buffer C (described above) and resuspended at 1×10^7/mL ice-cold CAR RPMI supplemented with 2mM EDTA. Cells were flow sorted using a BD FACS Aria (BD Biosciences) at the FACS Core Facility at the Medical University Innsbruck. For viability staining, 10µL 4′,6-diamidino-2-phenylindole (DAPI, 422801, 10.9M) was added to 1mL of cell suspension straight before acquisition. Viable EpCAM or EGFR positive tumor cells were directly sorted into DMEM+++ and seeded into T175 flasks (Szabo Scandic, 353112) immediately after sort. 1×10^5 viable $CD45^+$ CAR^+ T cells were directly sorted into 200µL RLT buffer (Qiagen, 74106) supplemented with 350mM 2-mercaptoethanol (bME, Sigma Adlrich, M3148) and 2.5µL RNAsin (Promega, N2515) in a RNAse-free 0.5mL Eppendorf tube, immediately frozen at dry ice and subsequently subjected to RNA isolation and bulk RNA sequencing (RNAseq).

Bulk RNAseq

For bulk RNAseq, total RNA was isolated using the RNeasy Micro kit (Qiagen, 74106) according to manufacturer's instructions. RNA was eluted in the kits elution buffer and stored at -80°C before quality control (QC). Purified total-RNA was submitted for transciptome analysis at the Medical University Innsbruck MultiOmics Sequencing Core for the purpose of gene-expression profiling, using the QuantSeq 3′ mRNA-Seq Library Prep method (Lexogen GmbH, Vienna Biocenter). Quality-validated, barcoded libraries were multiplexed and sequenced using Illumina NovaSeq technology (GeneWiz/Azenta, Leipzig, Germany).

Analysis of CAR-T cell bulk RNAseq

The nf-core/rnaseq (v3.14.0) [61] pipeline was used to align the raw reads to the mouse genome (GRCm39) with STAR and to assess the read counts on the gene models from GENCODE version M31 with Salmon. The pipeline was run using default parameters, but to accommodate the QuantSeq 3'-mRNA library data, the option '--extra_star_align_args' was modified as recommended in the documentation and '--noLengthCorrection' was used for gene quantification with Salmon [62]. DESeq (v1.42.1) was employed to identify differentially expressed genes between *Nr2f6*$^{-/-}$ CAR and WT CAR, applying a fold change threshold of 2 and a false discovery rate (FDR) of 0.1 after Independent Hypothesis Weighting (IHW) [63]. Enriched GO terms were calculated

using the R package topGO (v2.54.0) [64] and the significant differentially expressed genes (|log2foldchange| > 1, FDR < 0.1) as input. Enrichment scores were defined as -10 × log10(p.value_elim) and plotted as barplots. Pathway Gene set enrichment analysis (GSEA) was performed with the clusterProfiler [65] R package (v4.10.1) and the KEGG pathway database using genes ranked by the Wald statistic (stat) from DESeq2.

scTCRseq and scRNAseq analysis of CD45$^+$ tumor-infiltrating leukocytes from antigen-naïve recipients and *Nr2f6$^{crispr-/-}$* CAR-treated complete responder

Pre-processing of 10x VDJ and GEX sequencing files was performed with cellranger (v7.1.0) in the "cellranger multi" mode using the cellranger-vdj GRCm38 and gex-mm10-2020 reference files (10x Genomics). Raw count matrices were imported into AnnData and processed with scverse tools [66]. Ambient RNA was removed using scAR, and doublets were identified and removed using SOLO, both implemented in scvi-tools [67, 68]. Denoised count data underwent quality control in scanpy [69], involving two stages: 1. Pre-filtering: Cells were initially selected based on having more than 500 transcripts and over 200 genes. 2. Outlier removal: Cells showing excessive deviation (more than 5 times the median absolute deviation or MAD) in the number of transcripts, number of genes, or percentage of counts in the top 20% of genes were excluded. Additionally, cells with a high proportion of mitochondrial transcripts (deviating by more than 3xMAD or exceeding 8%) were also removed. Batch correction was performed as described above but "batch" (date of sample collection) was used as "batch_key" together with "donor" (individual animal) as "categorical_covariate_key". After unsupervised clustering with the Leiden algorithm, cell types were annotated based on known marker genes (see Suppl. Table 2 with marker genes). Pseudo-bulk profiles for each cell type were generated in Python with decoupler (git commit hash 9da10c9) summing up the counts and using the following filtering options: "min_cells=10" and "min_counts=1000". Differential expression analysis between responder (memory) and antigen-naïve samples was performed for each cell type using PyDESeq2 (v0.4.1) [70]. To examine which biological processes were enriched in the significant differentially expressed genes (|log2foldchange| > 1, p-adjusted < 0.1), gene ontology overrepresentation analysis was conducted using 'decoupler'. Dotplots were created in which the x-axis represents the 'combined score', calculated as the negative logarithm of the p-value multiplied by the odds ratio, providing a measure of the enrichment strength.

The TCRs were analyzed using the scirpy package (v0.13.1) [71]. Cells that did not have a full pair of receptor sequences were filtered out. Clonotypes were defined based on VJ and VDJ CDR3-sequence identity. As a metric for the TCR diversity and TCR clonality the normalized Shannon entropy and the Gini index respectively was calculated.

Statistical analysis

Statistical analysis was performed using GraphPad Prism software (v9.5.1). Data are represented as mean ± standard error of the mean (SEM) unless stated otherwise. Comparisons between two groups were calculated using two-tailed unpaired Student's t-test or non-parametric Mann-Whitney test as indicated in the figure legends. Comparisons between two or more groups with different variables were analyzed performing two-way ANOVA. In case of multiple comparison, the Šídák method was used. Bulk RNAseq and scRNAseq data were analyzed as stated above. Survival data was collected in a Kaplan-Meier curve and tested using log-rank tests. P-values <0.05 were considered significant. *$p \leq 0.05$, **$p \leq 0.01$, ***$p \leq 0.001$, ****$p \leq 0.0001$

Data availability

The bulk data generated in this study have been deposited in the Gene Expression Omnibus (GEO) under accession GSE284026 (https://www.ncbi.nlm.nih.gov/geo/query/acc.cgi?acc=GSE284026). The single-cell sequencing supporting the findings of this study are available on GEO and can be found with the accession GSE284026 (https://www.ncbi.nlm.nih.gov/geo/query/acc.cgi?acc=GSE284026). All data is publicly available and can be accessed by researchers worldwide. All data are included in the Supplementary Information or available from the authors, as are unique reagents used in this Article. The raw numbers for charts and graphs are available in the Source Data file whenever possible.

Code availability

While we did not develop any new algorithms or tools for this study, we did use a number of open source tools to analyze the data. The specific tools and versions that we used are listed in the methods section of the paper. We will share our analysis code upon request.

References

1. Labanieh L, Mackall CL. CAR immune cells: design principles, resistance and the next generation. *Nature* **614**, 635-648 (2023).

2. Labanieh L, Majzner RG, Mackall CL. Programming CAR-T cells to kill cancer. *Nat Biomed Eng* **2**, 377-391 (2018).

3. Maude SL*, et al.* Chimeric antigen receptor T cells for sustained remissions in leukemia. *N Engl J Med* **371**, 1507-1517 (2014).

4. Locke FL*, et al.* Axicabtagene Ciloleucel as Second-Line Therapy for Large B-Cell Lymphoma. *N Engl J Med* **386**, 640-654 (2022).

5. Park JH*, et al.* Long-Term Follow-up of CD19 CAR Therapy in Acute Lymphoblastic Leukemia. *N Engl J Med* **378**, 449-459 (2018).

6. Sotillo E*, et al.* Convergence of Acquired Mutations and Alternative Splicing of CD19 Enables Resistance to CART-19 Immunotherapy. *Cancer Discov* **5**, 1282-1295 (2015).

7. Orlando EJ*, et al.* Genetic mechanisms of target antigen loss in CAR19 therapy of acute lymphoblastic leukemia. *Nat Med* **24**, 1504-1506 (2018).

8. O'Rourke DM*, et al.* A single dose of peripherally infused EGFRvIII-directed CAR T cells mediates antigen loss and induces adaptive resistance in patients with recurrent glioblastoma. *Sci Transl Med* **9**, (2017).

9. Hirabayashi K*, et al.* Dual Targeting CAR-T Cells with Optimal Costimulation and Metabolic Fitness enhance Antitumor Activity and Prevent Escape in Solid Tumors. *Nat Cancer* **2**, 904-918 (2021).

10. Chan JD*, et al.* FOXO1 enhances CAR T cell stemness, metabolic fitness and efficacy. *Nature* **629**, 201-210 (2024).

11. Shi Y*, et al.* GLUT1 overexpression enhances CAR T cell metabolic fitness and anti-tumor efficacy. *Mol Ther*, (2024).

12. Ma L*, et al.* Vaccine-boosted CAR T crosstalk with host immunity to reject tumors with antigen heterogeneity. *Cell* **186**, 3148-3165 e3120 (2023).

13. Brossart P. The Role of Antigen Spreading in the Efficacy of Immunotherapies. *Clin Cancer Res* **26**, 4442-4447 (2020).

14. Kvistborg P*, et al.* Anti-CTLA-4 therapy broadens the melanoma-reactive CD8+ T cell response. *Sci Transl Med* **6**, 254ra128 (2014).

15. Awad MM*, et al.* Personalized neoantigen vaccine NEO-PV-01 with chemotherapy and anti-PD-1 as first-line treatment for non-squamous non-small cell lung cancer. *Cancer Cell* **40**, 1010-1026 e1011 (2022).

16. Kuhn NF, *et al.* CD40 Ligand-Modified Chimeric Antigen Receptor T Cells Enhance Antitumor Function by Eliciting an Endogenous Antitumor Response. *Cancer Cell* **35**, 473-488 e476 (2019).

17. Lai J, *et al.* Adoptive cellular therapy with T cells expressing the dendritic cell growth factor Flt3L drives epitope spreading and antitumor immunity. *Nat Immunol* **21**, 914-926 (2020).

18. Klampatsa A, Leibowitz MS, Sun J, Liousia M, Arguiri E, Albelda SM. Analysis and Augmentation of the Immunologic Bystander Effects of CAR T Cell Therapy in a Syngeneic Mouse Cancer Model. *Mol Ther Oncolytics* **18**, 360-371 (2020).

19. Hermann-Kleiter N, *et al.* The nuclear orphan receptor NR2F6 suppresses lymphocyte activation and T helper 17-dependent autoimmunity. *Immunity* **29**, 205-216 (2008).

20. Hermann-Kleiter N, *et al.* Nuclear orphan receptor NR2F6 directly antagonizes NFAT and RORgammat binding to the Il17a promoter. *J Autoimmun* **39**, 428-440 (2012).

21. Hermann-Kleiter N, *et al.* The Nuclear Orphan Receptor NR2F6 Is a Central Checkpoint for Cancer Immune Surveillance. *Cell Rep* **12**, 2072-2085 (2015).

22. Woelk J, Hornsteiner F, Aschauer-Wallner S, Stoitzner P, Baier G, Hermann-Kleiter N. Regulation of NK cell development, maturation, and antitumor responses by the nuclear receptor NR2F6. *Cell Death Dis* **16**, 77 (2025).

23. Jakic B, *et al.* Loss of the orphan nuclear receptor NR2F6 enhances CD8(+) T-cell memory via IFN-gamma. *Cell Death Dis* **12**, 187 (2021).

24. Klepsch V, *et al.* Nuclear receptor NR2F6 inhibition potentiates responses to PD-L1/PD-1 cancer immune checkpoint blockade. *Nat Commun* **9**, 1538 (2018).

25. Klepsch V, *et al.* Nuclear orphan receptor NR2F6 as a safeguard against experimental murine colitis. *Gut* **67**, 1434-1444 (2018).

26. Kim H, *et al.* Melanoma-intrinsic NR2F6 activity regulates antitumor immunity. *Sci Adv* **9**, eadf6621 (2023).

27. Karches CH, *et al.* Bispecific Antibodies Enable Synthetic Agonistic Receptor-Transduced T Cells for Tumor Immunotherapy. *Clin Cancer Res* **25**, 5890-5900 (2019).

28. Melenhorst JJ, *et al.* Decade-long leukaemia remissions with persistence of CD4(+) CAR T cells. *Nature* **602**, 503-509 (2022).

29. Shiqi L, *et al.* Durable remission related to CAR-T persistence in R/R B-ALL and long-term persistence potential of prime CAR-T. *Mol Ther Oncolytics* **29**, 107-117 (2023).

30. Escobar G, Mangani D, Anderson AC. T cell factor 1: A master regulator of the T cell response in disease. *Sci Immunol* **5**, (2020).

31. Utzschneider DT, *et al.* T Cell Factor 1-Expressing Memory-like CD8(+) T Cells Sustain the Immune Response to Chronic Viral Infections. *Immunity* **45**, 415-427 (2016).

32. Delgoffe GM*, et al.* The role of exhaustion in CAR T cell therapy. *Cancer Cell* **39**, 885-888 (2021).

33. Long AH*, et al.* 4-1BB costimulation ameliorates T cell exhaustion induced by tonic signaling of chimeric antigen receptors. *Nat Med* **21**, 581-590 (2015).

34. Zhang Z*, et al.* Gasdermin E suppresses tumour growth by activating anti-tumour immunity. *Nature* **579**, 415-420 (2020).

35. Hu Y*, et al.* The multifaceted roles of GSDME-mediated pyroptosis in cancer: therapeutic strategies and persisting obstacles. *Cell Death Dis* **14**, 836 (2023).

36. Utzschneider DT*, et al.* Early precursor T cells establish and propagate T cell exhaustion in chronic infection. *Nat Immunol* **21**, 1256-1266 (2020).

37. Hildner K*, et al.* Batf3 deficiency reveals a critical role for CD8alpha+ dendritic cells in cytotoxic T cell immunity. *Science* **322**, 1097-1100 (2008).

38. Kinkead HL*, et al.* Combining STING-based neoantigen-targeted vaccine with checkpoint modulators enhances antitumor immunity in murine pancreatic cancer. *JCI Insight* **3**, (2018).

39. Cheloni G*, et al.* Durable response to CAR T is associated with elevated activation and clonotypic expansion of the cytotoxic native T cell repertoire. *Nat Commun* **16**, 4819 (2025).

40. Sterner RC, Sterner RM. CAR-T cell therapy: current limitations and potential strategies. *Blood Cancer J* **11**, 69 (2021).

41. Li XN*, et al.* XCL1-secreting CEA CAR-T cells enhance endogenous CD8(+) T cell responses to tumor neoantigens to confer a long-term antitumor immunity. *J Immunother Cancer* **13**, (2025).

42. Mohamed AO*, et al.* CD4 T cell depletion increases memory differentiation of endogenous and CAR T cells and enhances the efficacy of Super2 and IL-33-armored CAR T cells against solid tumors. *J Immunother Cancer* **13**, (2025).

43. Wherry EJ*, et al.* Molecular signature of CD8+ T cell exhaustion during chronic viral infection. *Immunity* **27**, 670-684 (2007).

44. Bengsch B*, et al.* Epigenomic-Guided Mass Cytometry Profiling Reveals Disease-Specific Features of Exhausted CD8 T Cells. *Immunity* **48**, 1029-1045 e1025 (2018).

45. Guo X*, et al.* Global characterization of T cells in non-small-cell lung cancer by single-cell sequencing. *Nat Med* **24**, 978-985 (2018).

46. Miller BC*, et al.* Subsets of exhausted CD8(+) T cells differentially mediate tumor control and respond to checkpoint blockade. *Nat Immunol* **20**, 326-336 (2019).

47. Siddiqui I*, et al.* Intratumoral Tcf1(+)PD-1(+)CD8(+) T Cells with Stem-like Properties Promote Tumor Control in Response to Vaccination and Checkpoint Blockade Immunotherapy. *Immunity* **50**, 195-211 e110 (2019).

48. Sade-Feldman M*, et al.* Defining T Cell States Associated with Response to Checkpoint Immunotherapy in Melanoma. *Cell* **175**, 998-1013 e1020 (2018).

49. Bengsch B*, et al.* Bioenergetic Insufficiencies Due to Metabolic Alterations Regulated by the Inhibitory Receptor PD-1 Are an Early Driver of CD8(+) T Cell Exhaustion. *Immunity* **45**, 358-373 (2016).

50. Yu YR*, et al.* Disturbed mitochondrial dynamics in CD8(+) TILs reinforce T cell exhaustion. *Nat Immunol* **21**, 1540-1551 (2020).

51. Scharping NE*, et al.* Mitochondrial stress induced by continuous stimulation under hypoxia rapidly drives T cell exhaustion. *Nat Immunol* **22**, 205-215 (2021).

52. Vardhana SA*, et al.* Impaired mitochondrial oxidative phosphorylation limits the self-renewal of T cells exposed to persistent antigen. *Nat Immunol* **21**, 1022-1033 (2020).

53. Nikolos F*, et al.* Cell death-induced immunogenicity enhances chemoimmunotherapeutic response by converting immune-excluded into T-cell inflamed bladder tumors. *Nat Commun* **13**, 1487 (2022).

54. Wang-Bishop L*, et al.* Potent STING activation stimulates immunogenic cell death to enhance antitumor immunity in neuroblastoma. *J Immunother Cancer* **8**, (2020).

55. Warnecke M, Oster H, Revelli JP, Alvarez-Bolado G, Eichele G. Abnormal development of the locus coeruleus in Ear2(Nr2f6)-deficient mice impairs the functionality of the forebrain clock and affects nociception. *Genes Dev* **19**, 614-625 (2005).

56. Cadilha BL*, et al.* Combined tumor-directed recruitment and protection from immune suppression enable CAR T cell efficacy in solid tumors. *Sci Adv* **7**, (2021).

57. Lesch S*, et al.* T cells armed with C-X-C chemokine receptor type 6 enhance adoptive cell therapy for pancreatic tumours. *Nat Biomed Eng* **5**, 1246-1260 (2021).

58. Briukhovetska D*, et al.* T cell-derived interleukin-22 drives the expression of CD155 by cancer cells to suppress NK cell function and promote metastasis. *Immunity* **56**, 143-161 e111 (2023).

59. Brinkman EK, Chen T, Amendola M, van Steensel B. Easy quantitative assessment of genome editing by sequence trace decomposition. *Nucleic Acids Res* **42**, e168 (2014).

60. Lutz-Nicoladoni C*, et al.* Reinforcement of cancer immunotherapy by adoptive transfer of cblb-deficient CD8+ T cells combined with a DC vaccine. *Immunol Cell Biol* **90**, 130-134 (2012).

61. Ewels PA*, et al.* The nf-core framework for community-curated bioinformatics pipelines. *Nat Biotechnol* **38**, 276-278 (2020).

62. Patro R, Duggal G, Love MI, Irizarry RA, Kingsford C. Salmon provides fast and bias-aware quantification of transcript expression. *Nat Methods* **14**, 417-419 (2017).

63. Ignatiadis N, Klaus B, Zaugg JB, Huber W. Data-driven hypothesis weighting increases detection power in genome-scale multiple testing. *Nat Methods* **13**, 577-580 (2016).

64. Alexa A, Rahnenfuhrer J, Lengauer T. Improved scoring of functional groups from gene expression data by decorrelating GO graph structure. *Bioinformatics* **22**, 1600-1607 (2006).

65. Yu G, Wang LG, Han Y, He QY. clusterProfiler: an R package for comparing biological themes among gene clusters. *OMICS* **16**, 284-287 (2012).

66. Virshup I*, et al.* The scverse project provides a computational ecosystem for single-cell omics data analysis. *Nat Biotechnol* **41**, 604-606 (2023).

67. Gayoso A*, et al.* A Python library for probabilistic analysis of single-cell omics data. *Nat Biotechnol* **40**, 163-166 (2022).

68. Bernstein NJ, Fong NL, Lam I, Roy MA, Hendrickson DG, Kelley DR. Solo: Doublet Identification in Single-Cell RNA-Seq via Semi-Supervised Deep Learning. *Cell Syst* **11**, 95-101 e105 (2020).

69. Wolf FA, Angerer P, Theis FJ. SCANPY: large-scale single-cell gene expression data analysis. *Genome Biol* **19**, 15 (2018).

70. Bever KM*, et al.* The prognostic value of stroma in pancreatic cancer in patients receiving adjuvant therapy. *HPB (Oxford)* **17**, 292-298 (2015).

71. Sturm G*, et al.* Scirpy: a Scanpy extension for analyzing single-cell T-cell receptor-sequencing data. *Bioinformatics* **36**, 4817-4818 (2020).

Acknowledgements

This research was funded in part or in full by the Austrian Science Fund (FWF; Grant-DOI 10.55776/P31383 to GB, Grant-DOI 10.55776/P34368 to KBS, Grant-DOI 10.55776/PAT9292223 to TG and Grant-DOI10. 55776/T1292 to VK), the DOC fellowship from the Austrian Academy of Sciences to JK, the Bayerische Forschungsstiftung Grant BAYCELLATOR to SK and the European Research Council Fund (CoG 101124203 to SK, ADG 786462, PoC 101054365 and PoC 101189004, the last three to GB). We thank BMA Nina Posch and Dr. Friedrich Fresser (all from our institute in Innsbruck) for technical assistance. Illustrations in the figures were created with BioRender.com. For open access purposes, the author has applied a CC BY public copyright license to any accepted version of the manuscript arising from this submission.

Author contributions

D.H., V.K. and G.B. conceived and designed experiments. D.H., V.K., D.R., D.S., V.L., J.K., S.P., T.S., V.W., I.H., A.F., D.S., G.D., W.P., I.S., K.S., N.T., T.G. acquired data. D.R. performed bioinformatics analysis. D.H., V.K., D.R., D.S., G.D., W.P., N.T., T.G. and G.B. analyzed and interpreted data. D.H., V.K. and G.B. wrote the manuscript. A.K., S.S., S.K., Z.T., D.W., provided feedback. All authors read, revised

and approved the final manuscript.

Competing interests

SK has received honoraria from Cymab, Plectonic, TCR2 Inc., Miltenyi, Galapagos, Novartis, BMS and GSK. SK is an inventor of several patents in the field of immuno-oncology. SK received license fees from TCR2 Inc and Carina Biotech. SK received research support from TCR2 Inc., Tabby Therapeutics, Catalym GmBH, Plectonic GmBH and Arcus Bioscience for work unrelated to the manuscript. V.K., J.K., K.S., D.H. and G.B. are inventors on patents related to immunological targets in the field of immuno-oncology. D.R., I.H., D.S., V.L., S.P., T.S., Z.S., V.W., A.F., G.D., W.P., I-I. S., A.K., S.S., Z.T. and T.G. declare no competing interests.

FIGURE LEGENDS

Figure 1 *Nr2f6*-modified CAR-T cells confer superior anti-tumor immunity, achieving complete remission in a preclinical Panc02-EpCAM mouse model of solid tumors *in vivo*. A) Experimental CAR structure. scFv = single chain variable fragment. h = hinge. TM = transmembrane. IC = intracellular domain. Created in BioRender. Klepsch, V. (2026) https://BioRender.com/1s7z4s9. **B)** Experimental setup and timeline. Immunocompetent wild type mice were injected subcutaneously with 1×10^6 Panc02-EpCAM cells (mosaic: 71% EpCAM positive, 29% EpCAM negative) and treated 2 days later with 3.6×10^6 genetically modified 28ζ CAR-T cells using CRISPR/Cas9 (Non-targeting control/NTC vs $Nr2f6^{crispr\text{-}/\text{-}.g04}$). Created in BioRender. Humer, D. (2026) https://BioRender.com/egrvdww. Average tumor growth curve **(C)** and survival curve **(D)** and tumor growth in single mice **(E)**. Tumor area was compared to untreated tumor-bearing mice (PBS) and measured by caliper. 5 of 9 in the $Nr2f6^{crispr\text{-}/\text{-}.g04}$ CAR-T receiving cohort (n=9 mice) and 1 of 11 in the NTC CAR-T receiving cohort (n=11 mice) showed complete responses. 1 of 9 in the $Nr2f6^{crispr\text{-}/\text{-}.g04}$ CAR-T receiving cohort relapsed and had to be killed on day 100. PBS (n=9 mice), pooled from two independent experiments. **(F-J)** FACS analysis of NTC and $Nr2f6^{crispr\text{-}/\text{-}}$ CAR^+ T cells d3 after ACT in Panc02-EpCAM tumor-bearing mice. **(F)** Percentage of CAR T cells from total tumor digested cells. **(G)** gMFI of TCF-1 protein in CAR T cells in the draining lymph node. **(H)** Representative plot for TCF-1 protein expression. **(I+J)** CAR T cells from spleens were restimulated ex-vivo with Panc02-EpCAM cells and analyzed for intracellular cytokine (INFγ + GzmB) production by FACS. The experiments were done as two (C-E) biological replicates / one (F-J) biological replicate. (F-J) n=5 mice per genotype. Two-way ANOVA [C], Log-Rank test [D], two-tailed unpaired Student's t-test [F-J]. Data shown as mean ± SEM.

Figure 2 *Nr2f6* depletion in CAR-T cells improves cytotoxicity against Panc02-EpCAM tumor cells during chronic stimulation. (A) Flow cytometric analysis of CAR transduction efficiency in wild type and *Nr2f6*$^{-/-}$ CAR-T cells. Representative image shows 6 concatenated experiments per genotype; % CAR positive indicated in numbers. **(B)** IFNγ production after 24-hour co-culture with tumor cells 5 days after T cell isolation assessed by flow cytometry. Control and *Nr2f6*-deficient CAR-T cells were stimulated at an effector to target cell ratio of 5:1 with Panc02-EpCAM (100% positive). n = 5 replicates, derived from two independent experiments. **(C)** Experimental setup of chronic stimulation assay. Created in BioRender. Klepsch, V. (2026) https://BioRender.com/sespri5. **(D)** Cytotoxicity of control and *Nr2f6*-deficient CAR-T cells against GFP^{+} Panc02-EpCAM cells was assessed after serial stimulation, beginning five days after T cell isolation at E:T of 5:1 at 48-hour intervals in medium without cytokines. n = 9 replicates from four independent experiments, ns = 0.9536. Granzyme B **(E)** and IFNγ **(F)** release in the supernatant after each round of re-stimulation (every 48h) with GFP^{+} Panc02-EpCAM tumor cells beginning 5 days after T cell isolation assessed by Luminex xMAP technology. n = 6 replicates, derived from two independent experiments. **(G)** PCA blot from normalized RNAseq data obtained from wild type and *Nr2f6*$^{-/-}$ CAR-T cells isolated on d8 of serial killing (n = 3 per genotype, derived from one representative experiment). **(H)** Gene ontology (GO) terms of differential expressed genes showing significantly enriched pathways in *Nr2f6*$^{-/-}$ CAR-T cells compared to wild type control CAR-T cells isolated on day 8 of chronic stimulation. **(I)** Gasdermin E cleavage assay. Wild type and *Nr2f6*-modified CAR-T cells were chronically stimulated with Panc02-EpCAM tumor cells beginning on day five after T cell isolation at E:T 5:1. 6 hours after the 2nd re-stimulation, Panc02-EpCAM were analyzed for GSDME cleavage using immunoblot. Quantification was done in ImageJ. n = 6 replicates from two independent experiments. (B, I) Two-tailed unpaired Student's t test. (D) two-way ANOVA for each round. (E,F) multiple two-tailed unpaired Student's t test. Data shown as mean ± SEM. ns=not significant.

Figure 3 *Nr2f6*-modified CAR-T cells show an attenuated exhaustion phenotype during chronic stimulation. (A) Flow cytometric analysis of CD44 and CD62L expression on CAR-T cells on day 4 of chronic stimulation assay. n = 6 replicates from 2 independent experiments. **(B)** Representative image (d4) and ratio of progenitor (Tim3^{-}Ly108^{+}) to terminally (Tim3^{+}Ly108^{-}) exhausted T cells on d4 and d8 of chronic stimulation assay of wild type and *Nr2f6*$^{-/-}$ CAR-T cells.

n = 6 donors, from 2 independent experiments. Tpex = progenitor exhausted T cells; Ttex = terminally exhausted T cells; Text trans = transitory exhausted T cells. **(C)** Flow cytometric analysis of Tcf-1 expression in control and *Nr2f6*-deficient CAR-T cells on day 4 of chronic stimulation. Representative image (left) and quantification of geometric mean fluorescence intensity (gMFI) (right). n = 6 replicates from 2 independent experiments. (A+C) Two-tailed unpaired Student's t test. (B) two-sided non-parametric Mann-Whitney test. Data shown as mean ± SEM.

Figure 4 *Nr2f6* depletion in CAR-T cells maintains metabolic fitness during chronic stimulation. (A) Real-time mitochondrial stress test profile, oxygen consumption rate and **(B)** extra cellular acidification rate as measured by Seahorse Cell Mito Stress Test of control or *Nr2f6*-deficient CAR-T cells under resting and challenge conditions on day 4 of chronic stimulation. n = 6 donors in duplicates from two independent experiments. FCCP = Carbonyl cyanide p-trifluoro-methoxyphenyl hydrazone, AA+Rot = AntimycinA + Rotenone. (A) spare ns = p = 0.16, non mitoch. ns = p = 0.55. **(C)** PCA blot from normalized RNAseq data obtained from wild type and *Nr2f6*$^{-/-}$ CAR-T cells isolated on d4 of chronic stimulation (n = 3 replicates, data derived from one representative experiment). **(D)** Gene ontology (GO) terms obtained from overrepresentation analysis of differentially expressed genes RNAseq data showing significantly enriched pathways in *Nr2f6*$^{-/-}$ CAR-T cells compared to wild type control CAR-T cells. **(E)** Gene set enrichment analysis (GSEA) of *Nr2f6*-deficient CAR-T cells compared to control CAR-T cells isolated on 4 days of chronic stimulation using the KEGG database. Normalized enrichment scores (NES) and p values are shown. A positive NES indicates that the gene set was enriched in *Nr2f6*-deficient cells. (A+B) two-tailed unpaired Student's t-test, data shown as mean ± SEM, ns = not significant. (E) Wald statistic from DESeq2.

Figure 5 *Nr2f6*-modied CAR-T cells prime the endogenous immune system resulting in a secondary immune response against CAR-targeted and non-CAR-targeted antigens. (A) Experimental setup and timeline. Created in BioRender. Klepsch, V. (2026) https://BioRender.com/772xola. Average tumor growth curve **(B)** and survival curve **(C)** in

immunodeficient *Rag1*$^{-/-}$ recipient mice. *Rag1*$^{-/-}$ mice injected subcutaneously with 5 × 10^5 Panc02-EpCAM (100% positive) cells and treated 2 days later with 1 × 10^6 genetically modified 28ζ CAR-T cells using CRISPR/Cas9 (NTC vs *Nr2f6*$^{crispr-/-.g04}$ or *Nr2f6*$^{crispr-/-.g03}$). Tumor growth and survival was compared to the no therapy group that received PBS. Tumor volume was measured by caliper. n = 6 mice for *Nr2f6*$^{crispr-/-g03}$ and PBS and n = 5 mice for NTC and *Nr2f6*$^{crispr-/-.g04}$, representative of two independent experiments. (B) two-way ANOVA *Nr2f6*$^{crispr-/-.g04}$ vs. *Nr2f6*$^{crispr-/-.g03}$: ns = p = 0.9889, (C) overall ns = p = 0.2295, PBS vs *Nr2f6*$^{crispr-/-.g04}$ ns = p = 0.1213. **(D)** Experimental setup and timeline for FACS and ELISpot analysis. Ly5.1 mice were used as recipients to track Ly5.2 NTC or *Nr2f6*$^{crispr-/-.g03}$ CAR-T cells. Created in BioRender. Klepsch, V. (2026) https://BioRender.com/oeq94aw. **(E)** Flow cytometric analysis of splenocytes from three NTC and three *Nr2f6*$^{crispr-/-.g03}$ CAR-T cell-treated wild type tumor-bearing mice on d8 after tumor inoculation (1 × 10^6 Panc02-EpCAM^{mosaic}). Increased proportion of cDC1 in *Nr2f6*$^{crispr-/-.g03}$ CAR T cell treated animals compared to NTC. cDC1 were gated as exemplified in Suppl.Fig.7A, n = 3 mice per group. **(F)** IL12p40 concentration in serum of NTC and *Nr2f6*$^{crispr-/-}$ CAR T treated tumor-bearing mice d6 after ACT determined by LUMINEX technology. Data was normalized to NTC CAR T receiving mice. n = 2 PBS, 3 NTC CAR, and 6 *Nr2f6*$^{crispr-/-}$ CAR mice. **(G, H)** Granzyme B ELISpot assay. Immunocompetent wild type mice were injected subcutaneously with 1 × 10^6 Panc02-EpCAM^{mosaic} cells and left untreated (PBS) or treated 2 days later with 3.6 × 10^6 genetically modified 28ζ NTC or *Nr2f6*$^{crispr-/-.g03}$ CAR-T cells. Assay was performed with isolated endogenous CD3$^+$ T cells on day 21 after tumor inoculation. NTC versus *Nr2f6*$^{crispr-/-.g03}$ CAR-T. n = 5 mice per group from 2 independent experiments. (E-G) two-tailed unpaired Student's t-test. Data shown as mean ± SEM.

Figure 6 *Nr2f6*-modified CAR-T cell-treated complete responders exert a durable immune memory protection against CAR-targeted antigen-positive and CAR-targeted antigen-negative Panc02 tumors. (A) Experimental setup and timeline. Created in BioRender. Humer, D. (2026) https://BioRender.com/bcyeh6x. **(B)** Average tumor growth and **(C)** survival curve. Tumor growth and survival of NTC and *Nr2f6*$^{crispr-/-.g04}$ CAR-T cell receiving complete responders (CR) re-challenged 150 days with 2.5 × 10^6 Panc02-EpCAM^{pos} (left flank) and 1 × 10^6 Panc02-EpCAM^{neg} (right flank) tumor cells (1st re-challenge). Naïve, age-matched C57BL/6 mice were used as controls (naïve wild type). n = 4 for *Nr2f6*$^{crispr-/-.g04}$ CR, n = 1 for NTC CR and n = 7 for

naïve WT from one memory experiment. CR = complete responders, (B) Panc02-EpCAM^{hi} ns = p = 0.385, Panc02-EpCAM^{neg} ns = p = 0.680. **(D-E)** *Nr2f6$^{crispr-/-.g04}$* CAR-T cell-treated long-term CR received a 2nd re-challenge 150 days later (300 days after initial tumor induction) with 1 × 10^6 Panc02-EpCAM^{neg} tumor cells. Naïve age-matched C57BL/6 mice were used as controls (naïve wild type) **(D)** Tumor growth and survival of Panc02-EpCAM^{neg}-naïve (1 × 10^6) tumor-bearing wild type mice adoptively transferred with 1 × 10^7 splenocytes from 2nd re-challenged CR euthanized on d305 or Panc02-naïve splenocytes. n = 8 for naïve splenocytes, and n = 7 for *Nr2f6$^{crispr-/-.g04}$* CR splenocytes. **(E)** Flow cytometric analysis of IFNγ production after 24-hour co-culture of CD8 T cells from CR with tumor cells. Naïve and CR were stimulated at E:T of 5:1 with Panc02-EpCAM^{pos} tumor cells. n = 4 from two independent experiments. EpCAM^{pos} = EpCAM positive, EpCAM^{neg} = EpCAM negative.(B+D) Two-way ANOVA with Šídák's multiple comparisons test, (C+D) Log-rank rest (E) two-tailed unpaired Student's t-test. Data are presented as mean ± SEM.

Figure 7 *Nr2f6*-modified CAR-T cells treated complete responders trigger a high-quality secondary and polyclonal immune response assessed by scRNA- and scTCRseq. (A) UMAP plots showing cell annotation for naïve vs. CR mice. CD45$^+$ TILs from tumor-bearing *Nr2f6*-modified CAR-T cell-treated CR and Panc02-naïve mice were subjected to scRNA- and scTCRseq. CR = complete responder **(B)** Stacked charts showing proportions of each cell cluster **(C, D)** ORA of GO terms showing enriched pathways in intratumoral proliferating CD8 T cells and cDC1. **(E)** TCR scRNA-seq; Gini index of TCR clonality (p=0.20) and Shannon entropy of diversity (p=0.34) were compared in naïve and CR tumor-bearing mice. (A-E) n = 4 per group (naïve vs CR), one representative experiment. **Graphical Summary: Functional advantages and mechanisms underlying *Nr2f6*-modified CAR-T cell therapy in a solid tumor model. F. *In vitro*:** Conventional CAR-T cells exhibit reduced cytotoxicity, impaired cytokine release, increased exhaustion, and diminished metabolic fitness. In contrast, *Nr2f6*-modified CAR-T cells display enhanced tumor-cell killing, increased IFNγ and TNFα production, and improved metabolic performance under repetitive stimulation. **G. *In vivo*:** Schematic depiction of therapeutic dynamics following CAR-T cell infusion into solid tumor-bearing mice. Conventional CAR-T cells progressively lose efficacy due to antigen heterogeneity, immunosuppressive cues within the

tumor microenvironment (TME), and cumulative dysfunction. In comparison, *Nr2f6*-modified CAR-T therapy induces immunogenic tumor cell death (ICD), facilitates antigen uptake and presentation by host antigen-presenting cells (APCs), and immune responses beyond the initial CAR target. **H. Overall concept:** The major limitations of conventional CAR-T cells in solid tumors, antigen heterogeneity, a suppressive TME, and limited persistence, are overcome by *Nr2f6*-modified CAR-T cells. These cells retain sustained cytotoxic activity, effectively target heterogeneous tumor antigens, and provoke a durable, polyclonal host immune memory response. For the first time, this approach demonstrates that antigenically diverse solid tumors can be efficiently eradicated, bridging the efficacy gap between hematologic and solid malignancies in CAR-T therapy. All schematics are conceptual representations summarizing the cellular and molecular events that collectively underlie the enhanced therapeutic efficacy of *Nr2f6*-modified CAR-T cells. Created in BioRender. Klepsch, V. (2026) https://BioRender.com/sezlqdw.

Editor's Summary
Efficacy of chimeric antigen receptor (CAR)-T in solid tumors are limited by the antigen heterogeneity and tumor microenvironment (TME) induced exhaustion. The authors here manifested that NR2F6 deficient CAR-T cells have superior anti-tumor effect compared with traditional CAR-T cells, which is associated with enhanced cytotoxic function, followed by durable response due to epitope spreading.

Peer review information: *Nature Communications* thanks Martín Bonamino who co-reviewed with Emmanuel Aragão; and the other anonymous reviewer(s) for their contribution to the peer review of this work. A peer review file is available.

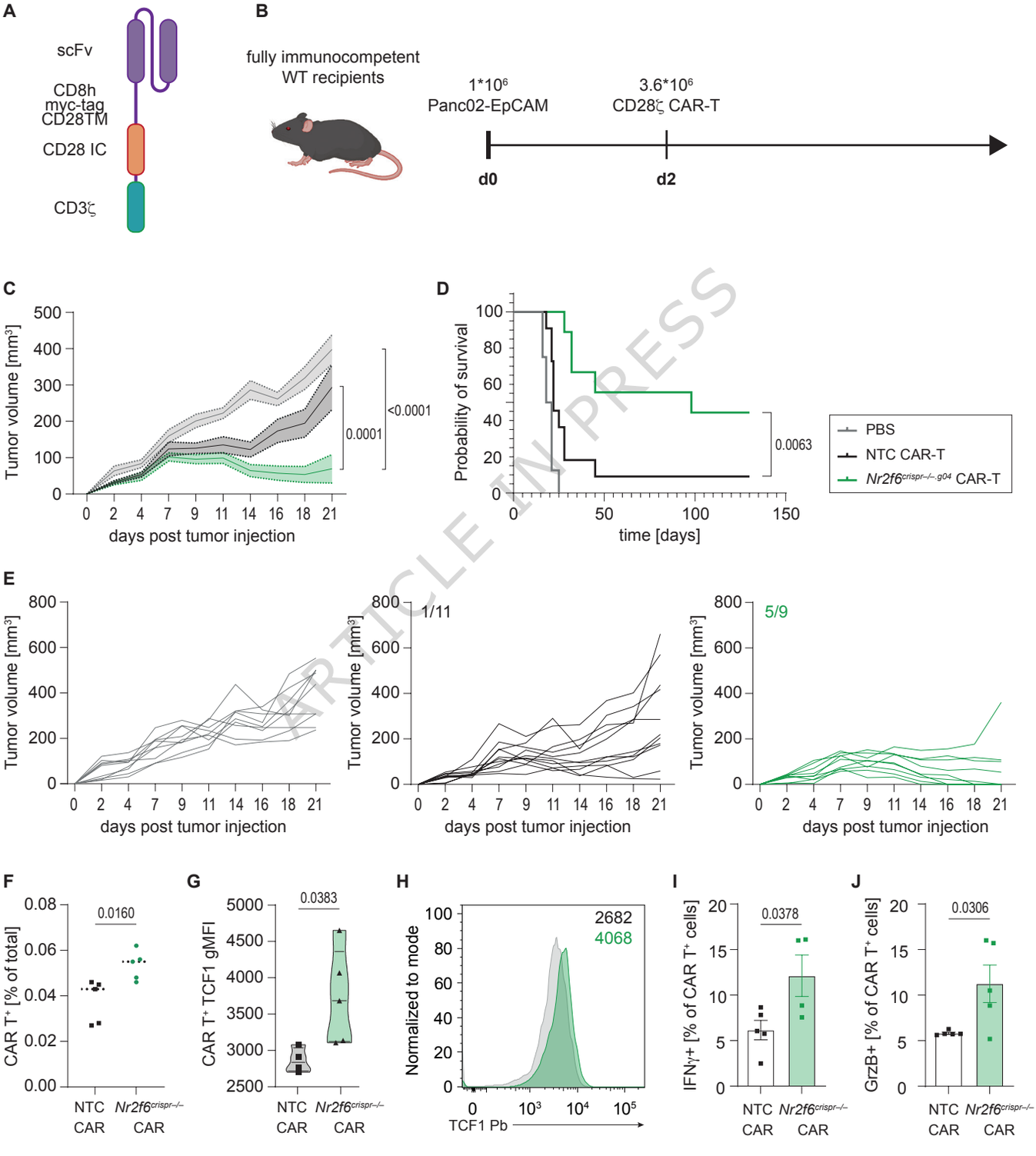

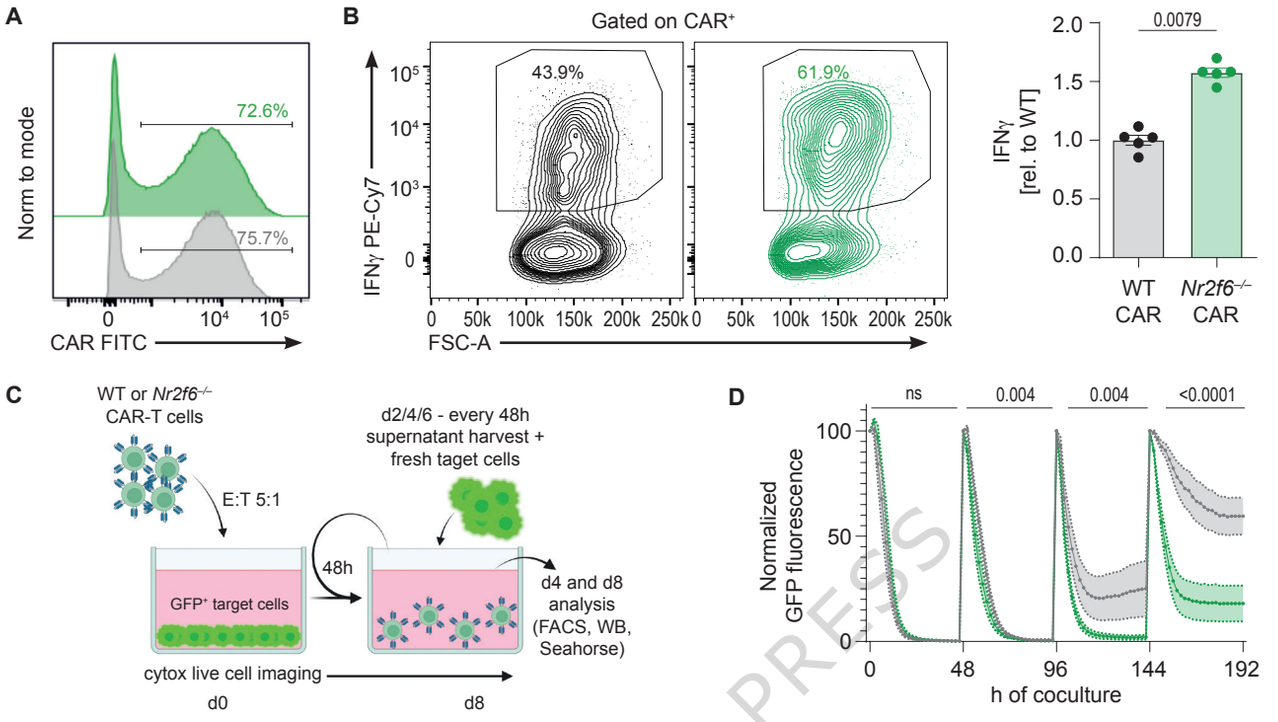

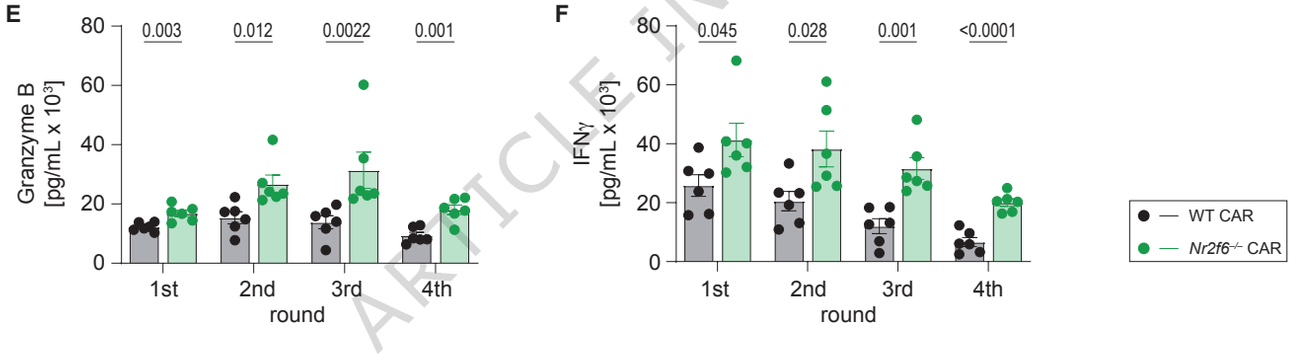

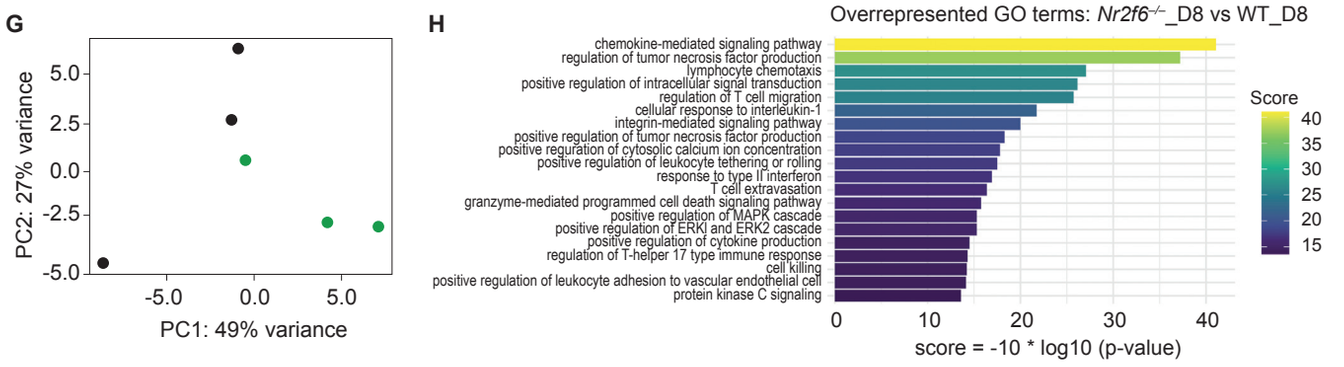

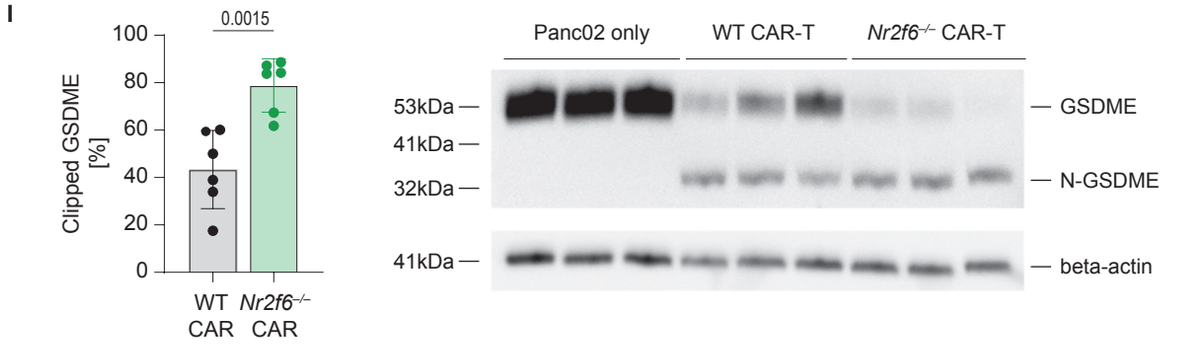

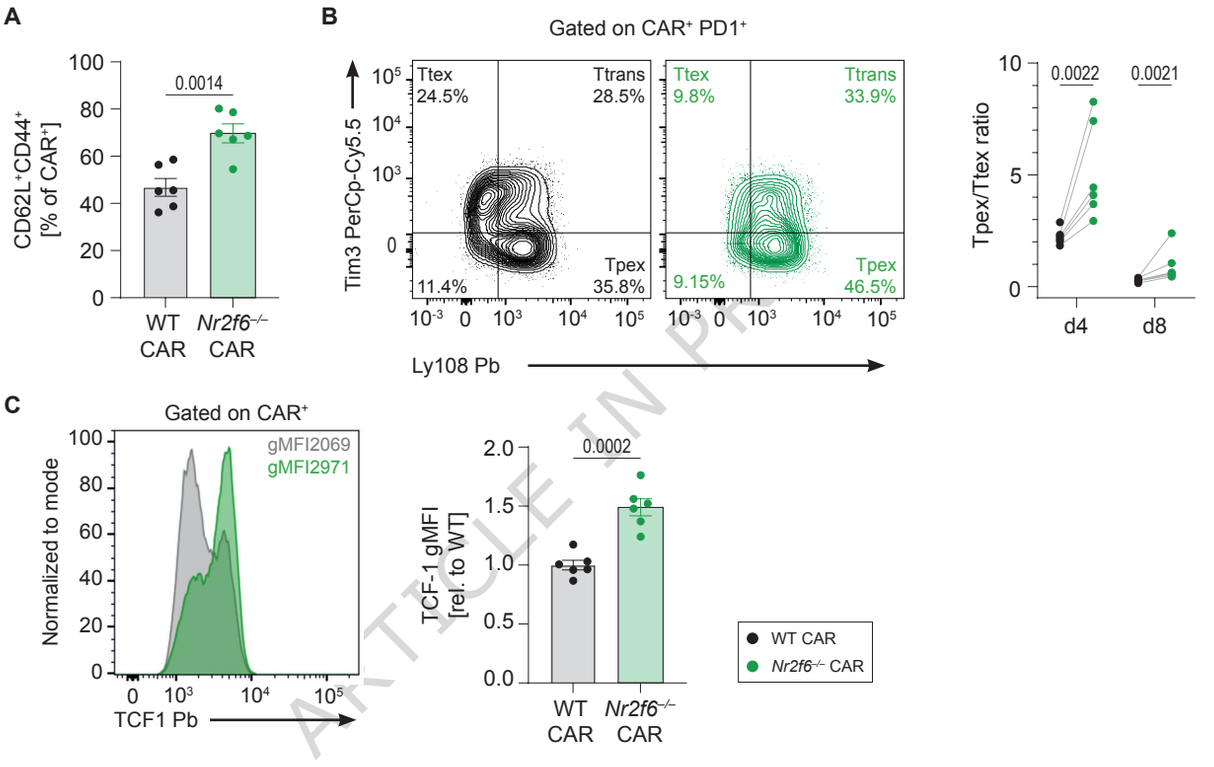

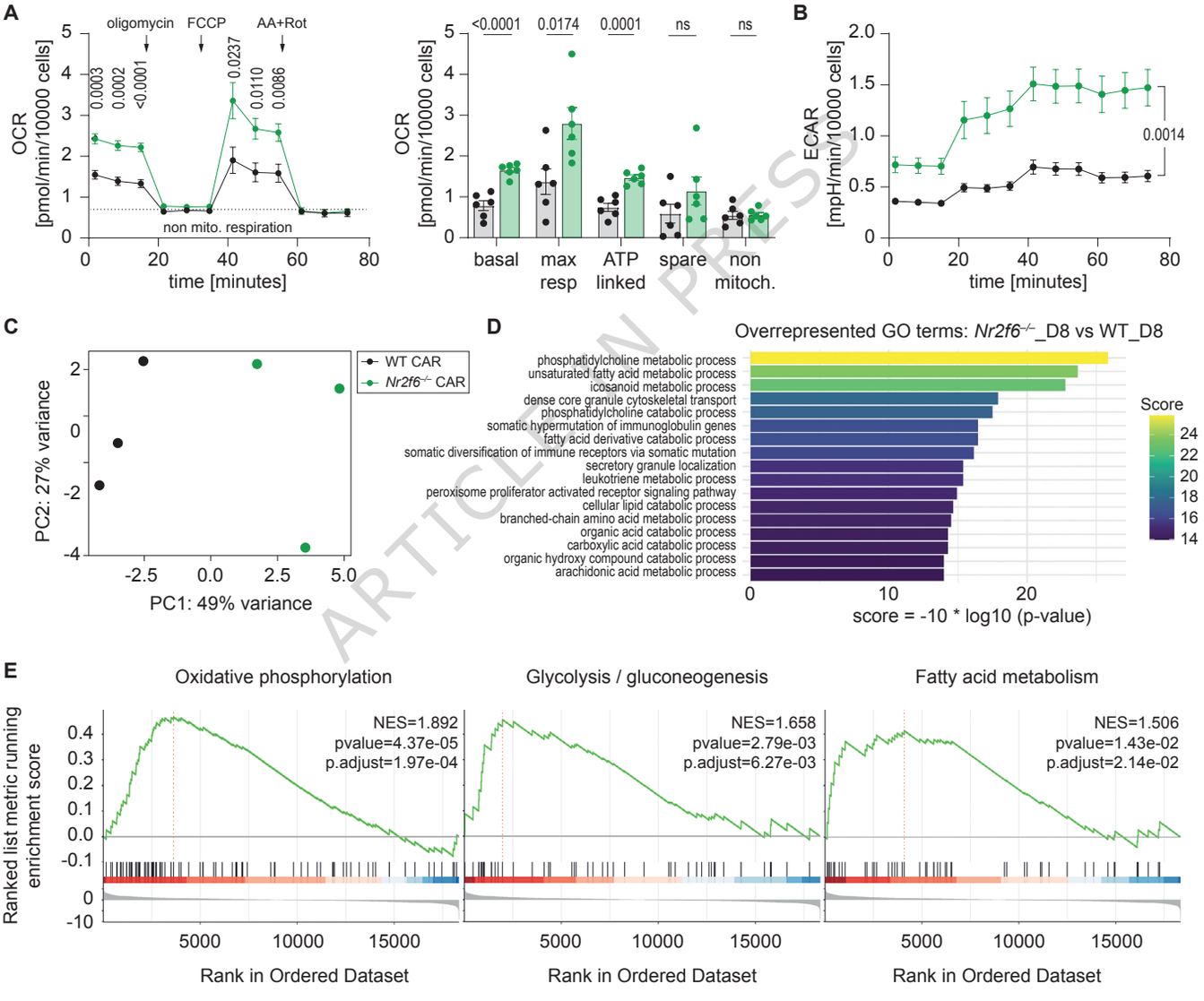

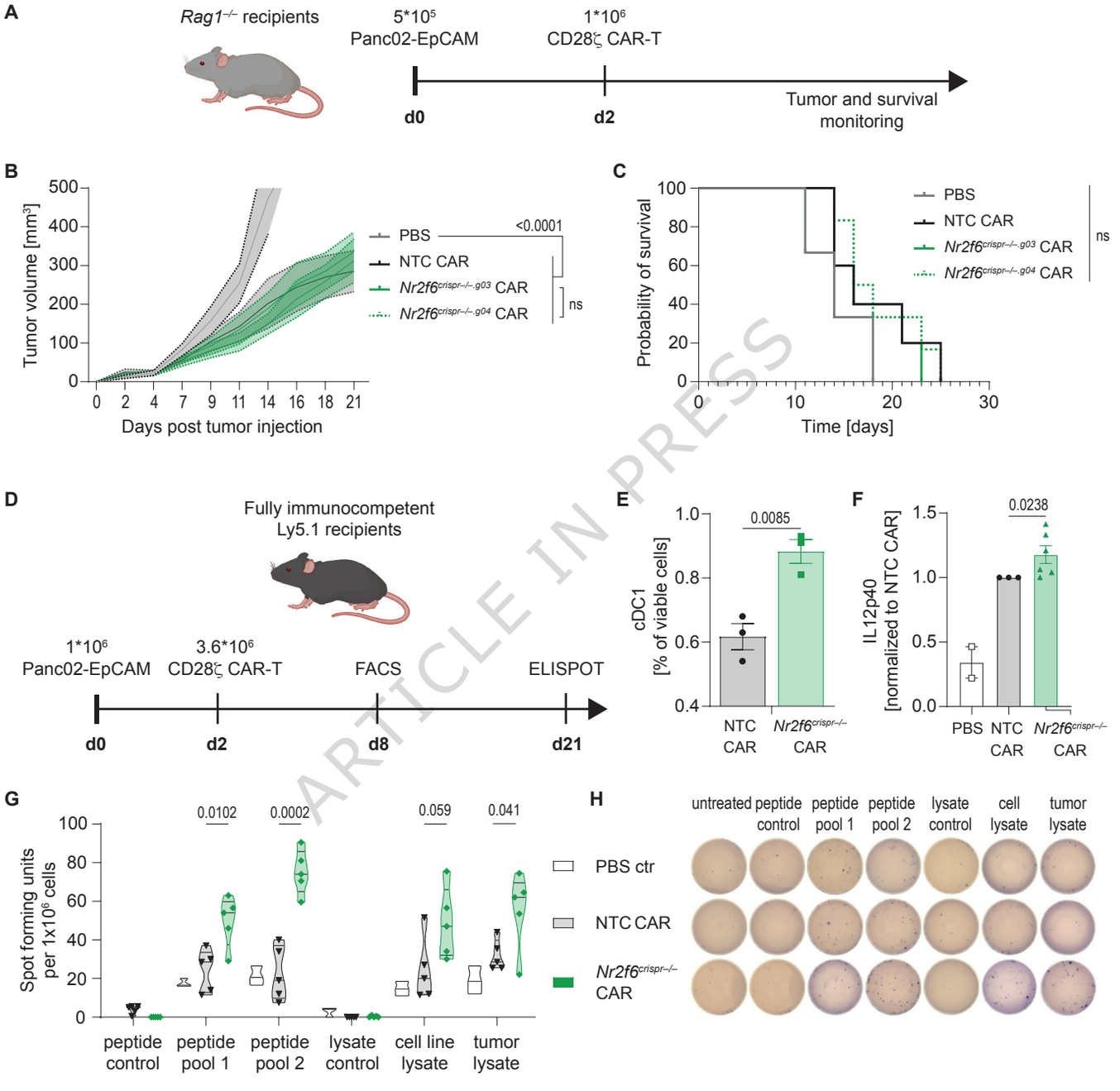

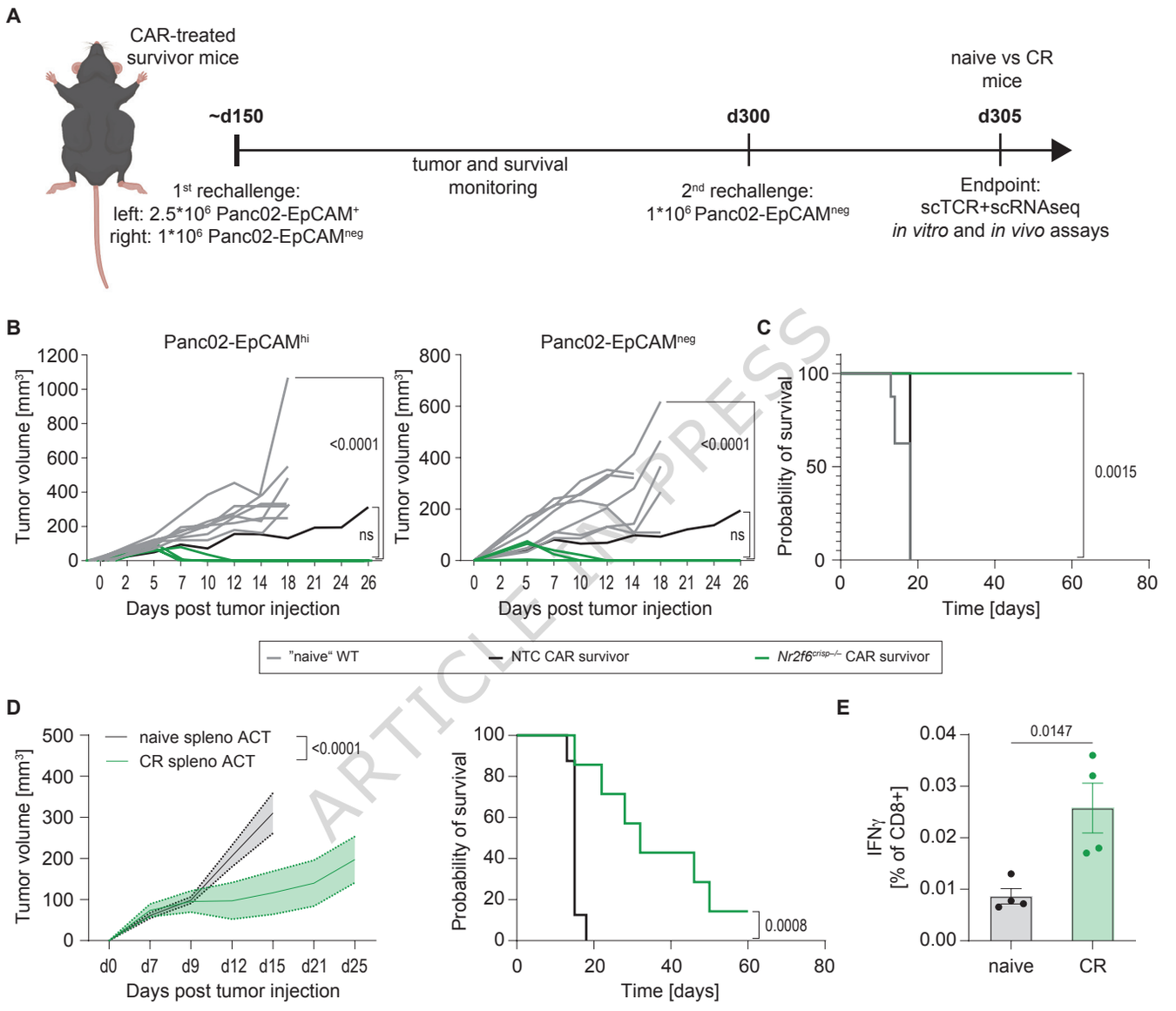

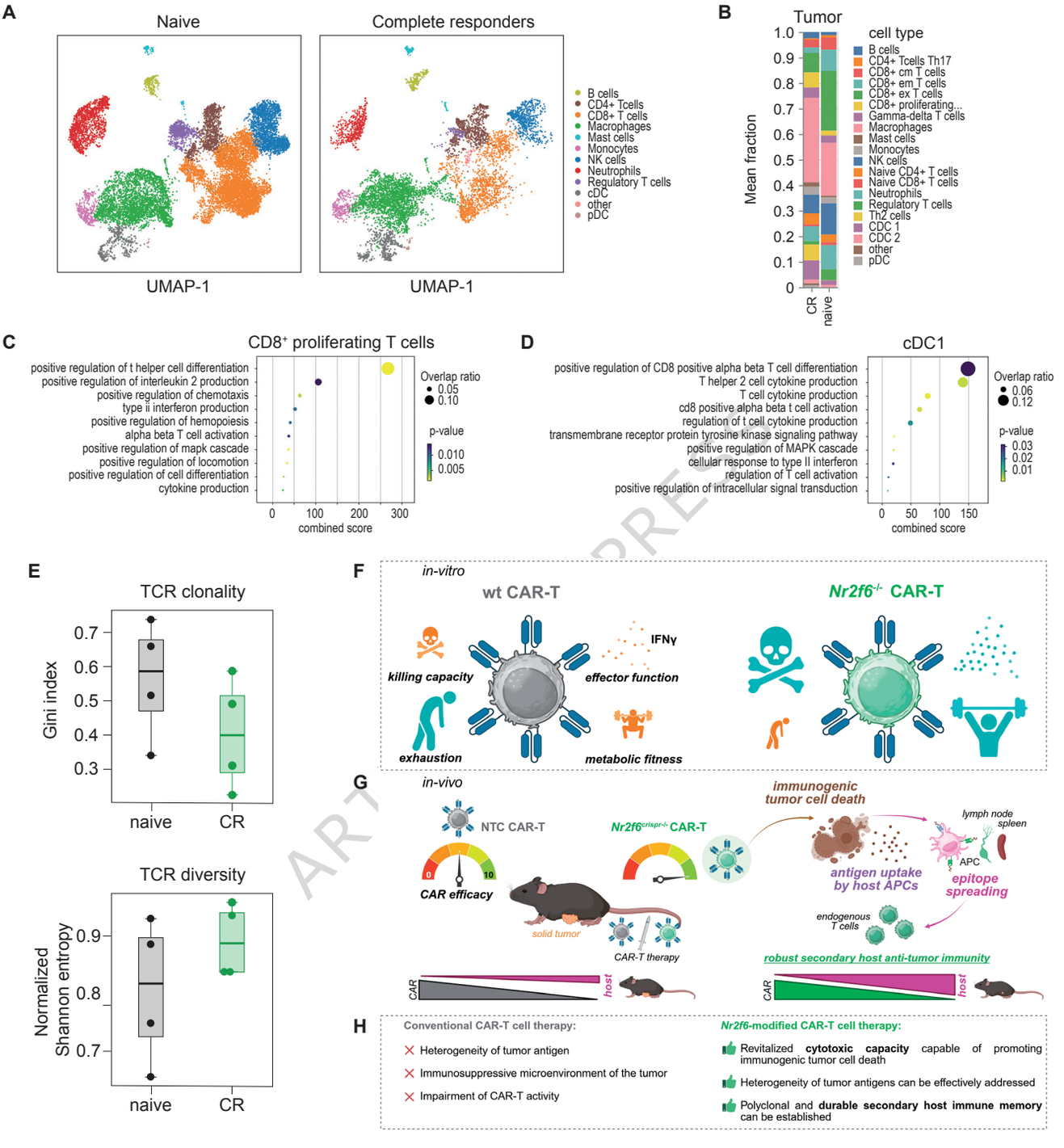
A
Naive
Complete responders
UMAP-1
UMAP-1
B cells
CD4+ Tcells
CD8+ T cells
Macrophages
Mast cells
Monocytes
NK cells
Neutrophils
Regulatory T cells
cDC
other
pDC
B
Tumor
Mean fraction
CR
naive
cell type
B cells
CD4+ Tcells Th17
CD8+ cm T cells
CD8+ em T cells
CD8+ ex T cells
CD8+ proliferating...
Gamma-delta T cells
Macrophages
Mast cells
Monocytes
NK cells
Naive CD4+ T cells
Naive CD8+ T cells
Neutrophils
Regulatory T cells
Th2 cells
CDC 1
CDC 2
other
pDC
C
CD8⁺ proliferating T cells
positive regulation of t helper cell differentiation
positive regulation of interleukin 2 production
positive regulation of chemotaxis
type ii interferon production
positive regulation of hemopoiesis
alpha beta T cell activation
positive regulation of mapk cascade
positive regulation of locomotion
positive regulation of cell differentiation
cytokine production
combined score
Overlap ratio
p-value
D
cDC1
positive regulation of CD8 positive alpha beta T cell differentiation
T helper 2 cell cytokine production
T cell cytokine production
cd8 positive alpha beta t cell activation
regulation of t cell cytokine production
transmembrane receptor protein tyrosine kinase signaling pathway
positive regulation of MAPK cascade
cellular response to type II interferon
regulation of T cell activation
positive regulation of intracellular signal transduction
combined score
Overlap ratio
p-value
E
TCR clonality
Gini index
naive
CR
TCR diversity
Normalized Shannon entropy
naive
CR
F
in-vitro
wt CAR-T
Nr2f6-/- CAR-T
killing capacity
IFNγ
effector function
exhaustion
metabolic fitness
G
in-vivo
NTC CAR-T
Nr2f6crispr-/- CAR-T
CAR efficacy
solid tumor
CAR-T therapy
immunogenic tumor cell death
lymph node
spleen
APC
antigen uptake by host APCs
epitope spreading
endogenous T cells
robust secondary host anti-tumor immunity
CAR
host
H
Conventional CAR-T cell therapy:
Heterogeneity of tumor antigen
Immunosuppressive microenvironment of the tumor
Impairment of CAR-T activity
Nr2f6-modified CAR-T cell therapy:
Revitalized cytotoxic capacity capable of promoting immunogenic tumor cell death
Heterogeneity of tumor antigens can be effectively addressed
Polyclonal and durable secondary host immune memory can be established